

Swimming in Complex Fluids

Saverio E. Spagnolie¹ and Patrick T. Underhill,²

¹Department of Mathematics, and Department of Chemical and Biological Engineering, University of Wisconsin-Madison, Madison, WI, USA, 53706; email: spagnolie@math.wisc.edu

²Department of Chemical and Biological Engineering, Rensselaer Polytechnic Institute, Troy, NY, USA, 12180; email: underhill@rpi.edu

Xxxx. Xxx. Xxx. Xxx. YYYY. AA:1–31

[https://doi.org/10.1146/\(\(please add article doi\)\)](https://doi.org/10.1146/((please add article doi)))

Copyright © YYYY by Annual Reviews.
All rights reserved

Keywords

swimming, locomotion, complex fluids, soft matter, active matter, active suspensions, biological fluids

Abstract

We review the literature on swimming in complex fluids. A classification is proposed by comparing the length and time scales of a swimmer with those of nearby obstacles, interpreted broadly, extending from rigid or soft confining boundaries to molecules which confer the bulk fluid with complex stresses. A third dimension in the classification is the concentration of swimmers, which incorporates fluids whose complexity arises purely by the collective motion of swimming organisms. For each of the eight system classes which we identify we provide a background and describe modern research findings. While some classes have seen a great deal of attention for decades, others remain uncharted waters still open and awaiting exploration.

1. INTRODUCTION

Biological fluids are messy. They can become more or less viscous by stirring them. They can store and release elastic energy across a wide range of relaxation timescales, or they can be soft in one direction and hard in another. Strange as they may be, these are the environments that microorganisms must often navigate in order to survive. A medium can even express astounding bulk features due to the emergent activity of the microorganisms themselves. The scientific literature on swimming in complex fluids is equally expansive - the phrase itself is used to describe physical systems which may seem hardly related.

The physics of swimming has captured the imagination for millenia (1), but advanced theories treating the locomotion of bodies through fluids would not appear until the dawn of mathematical fluid mechanics, and then the confluence of physics and biology in the 20th century. The study of microorganism locomotion at the micron scale, where viscous dissipation dominates inertia, has now been a tremendously active research area for the better part of a century (2–6).

The earliest works produced a great understanding of swimming in idealized (“Newtonian”) fluids. The fluids through which microorganisms swim, however, are often endowed with highly nonlinear, non-Newtonian features when viewed at a continuum scale, including shear-dependent viscosity, elasticity, and other features which blur the lines between fluids and solids. A broader understanding of the role of complex fluids in biological systems, including and beyond the physics of locomotion, is achieved with each passing year (7). The importance of these complex fluid phenomena on self-propulsion depends on the length- and time-scales of the body motion when compared to those of the environment. Just as the Reynolds number¹ measures the relative importance of inertial and viscous effects, so the Carreau, Weissenberg, Bingham, and Ericksen numbers measure the importance of shear-thinning, viscoelasticity, viscoplasticity, and anisotropy (10).

Some fluids are even complex *as a consequence* of microorganism activity if treating the suspension of swimmers as part of the material. Active suspensions or active matter can exhibit orientational order and elastic response, shear-dependent viscosity, and “negative viscosity” (11–15). In addition to the microorganisms and suspending material, the presence of boundaries, whether internal to the fluid or confining it externally, can contribute to the emergence of the complex features noted above. For a broader look at the literature on confinement of active particles see the review by Bechinger et al. (16).

Given the many interpretations and dimensions of “swimming in complex fluids” a classification system would seem to be of use. Such a system may help identify the most important features of a physical system and unify seemingly disparate effects. The purpose of this review is twofold. First we aim to outline such a classification for swimming in complex fluids. To identify distinct classes we will consider the relationship of the swimmer(s) to the constituents or obstacles that provide the fluid with complex features through their relative lengths and timescales, and consider the concentration of swimmers. The second goal of this paper is to provide a review of the literature for each of these classes, and to draw connections between them. While our classification is not all-encompassing, we hope that it will provide organizational clarity on the tremendously diverse field of physical phenomena and biological behavior.

¹The Reynolds number, $Re = \rho UL/\mu$, with μ the fluid’s viscosity, and L and U characteristic length and velocity scales of the swimming body, is orders of magnitude smaller than 1 for microorganism locomotion (8, 9).

2. A CLASSIFICATION OF SWIMMING IN COMPLEX FLUIDS

It was the misfortune of the Proteus and her crew to be pioneers into a realm that was literally unknown; surely a fantastic voyage if ever there was one. (17)

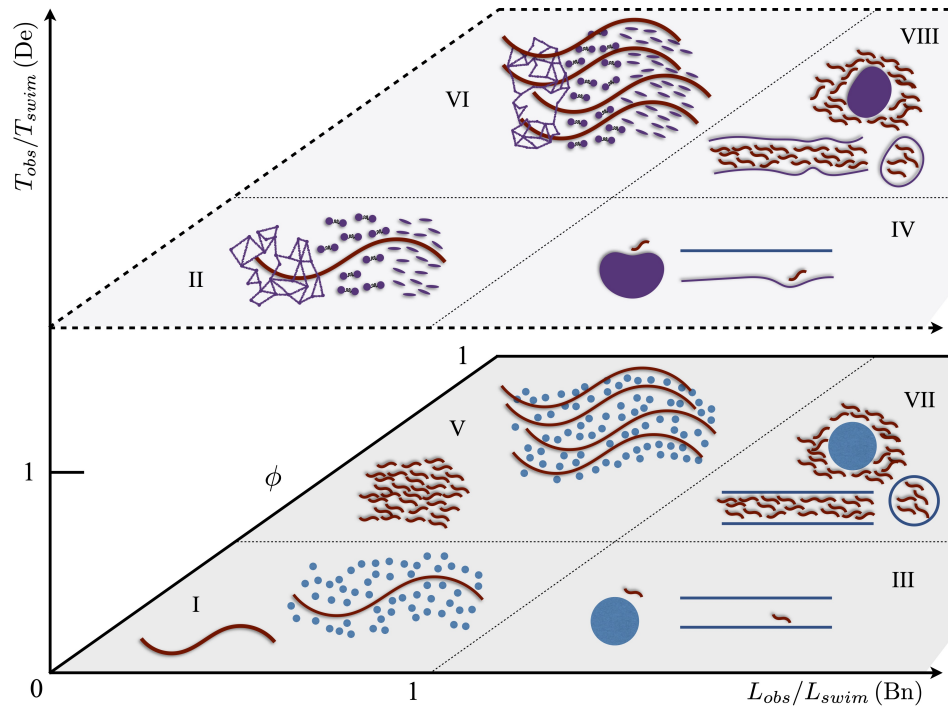


Figure 1

A classification of swimming in complex fluids. The axes are the relative lengths of the obstacle(s) to the swimmer, $Bn = L_{obs}/L_{swim}$, their relative timescales, $De = T_{obs}/T_{swim}$, and the volume fraction of swimmers ϕ . Red objects are active (swimming), blue objects are rigid, and purple objects are deformable. I/II: a single swimmer in a suspension of small rigid/deformable obstacles; III/IV: a single swimmer near a large rigid/deformable obstacle; V/VI: many swimmers in a suspension of small rigid/deformable obstacles; VII/VIII: many swimmers near a large rigid/deformable obstacle.

With the aim of organizing the complex fluid phenomena which either affect or are caused by swimming microorganisms, we focus on the relationship between an individual swimmer and its environment. The environment is characterized by the distribution and behavior of “obstacles”, broadly interpreted. There may be only one large obstacle, representing a rigid or deformable boundary. Or the obstacles might be much smaller than the swimming body, like polymers or long-chain proteins, which relax into their preferred configurations over an intrinsic set of timescales. When there are sufficiently many such obstacles they confer the fluid with bulk features like viscoelasticity and shear-dependent viscosity. The obstacles might move with a background fluid, might themselves compose the background fluid, or they might be nearly fixed in space, for example if the obstacle is

large or if it is composed of a cross-linked network of fibers.

Figure 1 shows eight extremes of interest in our classification system, organized in a three-dimensional space. The vertical axis is the relaxation timescale of the obstacle(s) relative to a timescale associated with swimming motion, T_{obs}/T_{swim} , often called the Deborah number, De (18). Depending on the context and the physical processes that produce the timescales, this ratio might instead be referred to as a Weissenberg number, or possibly by other names, as will be discussed. The horizontal axis is the length scale of the obstacle(s) relative to a length associated with the swimming body, L_{obs}/L_{swim} , which we term the Benes number², Bn . Finally the third axis is the volume fraction of swimmers, ϕ . The location of a system in this three-dimensional space influences the relative importance of different effects and the behaviors observed, and from a mathematical perspective the modeling approximations which are most appropriate. The ratio of length scales and concentrations determines whether the swimmers or obstacles appear as an effective continuum. The ratio of frequencies or time scales determines the extent to which the suspending medium’s relaxation properties affect the dynamics. The concentration of swimmers determines the importance of interactions among groups of swimmers or active particles.

The classification is not all-encompassing, and there are physical systems which could lie in multiple domains or sit outside of it altogether. For instance, an additional time scale (and classification axis) not considered here is associated with the rate of viscous dissipation and determines the relative importance of inertia. Nevertheless we press on to discuss some of the fundamental features of the proposed organization. We begin with Type I systems, which at the extreme includes a single swimmer in a Newtonian fluid.

\mathcal{I} . Small De , small Bn , small ϕ : a single swimmer and small rigid obstacles

In Type I systems, a single swimmer navigates an environment containing small obstacles which are effectively rigid on the timescale of swimming. At the extreme separation of length scales, far to the right in **Figure 1**, the obstacles might even be the fluid constituents at the molecular scale; taking 10 microns as a characteristic swimmer size and comparing to the size of a single water molecule, $Bn \approx 10^{-3}$. Type I therefore includes swimming in classical Newtonian fluids, a familiar territory from which to depart on our journey.

The pioneering work on self-propulsion in viscous fluids appeared alongside improvements in microscope technology in the 1950s-1970s. Mathematical theories revealed many key features of swimming in Newtonian fluids at the microscale. They include instantaneously force- and torque-free dynamics, viscosity-independent swimming speeds for fixed gaits, kinematic reversibility (the “Scallop theorem” (8)), and widespread use of slender filament drag anisotropy (3, 5, 9, 19). Mathematical models from this era which remain mainstays across the field include Taylor’s infinite swimming sheet (20), Lighthill and Blake’s spherical envelope squirmer (21) and rotating helical model flagella (2).

Moving away from the origin and this Newtonian extremity, the rigid obstacles in question increase in size relative to the swimmer size. If still small compared to the swimmer but large compared to the fluid’s molecular constituents, they may still contribute features

²In the fictional “Fantastic Voyage” by Jerome Bixby and Otto Klement, novelized by Isaac Asimov, Dr. Jan Benes perfects a technology to manipulate an object’s size (17). His body’s various complex fluids go on to pose swimming and other challenges to the miniaturized crew injected into him to save his life.

to the fluid which the swimmer experiences as a change in the bulk rheology. A porous medium, for example, which strongly affects the relationship between pressure and flow can in turn have an effect on a relatively large swimming body. **Figure 2a** shows the velocity magnitude of a flow past a rigid cylinder in a model porous (Brinkman) fluid, suggestive of a particularly strong drag anisotropy. Such an environment was found to enhance undulatory and helical self-propulsion (22, 23). But decreased speeds were observed in the same medium for soft, deformable swimmers (22, 23) and for model tangential squirmers (24).

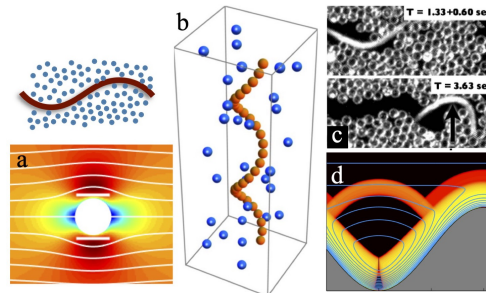


Figure 2

Type I systems. (a) Velocity magnitude of flow past a cylinder and streamlines in a model porous (Brinkman) medium - the additional anisotropy results in enhanced swimming speeds (22). (b) A helical filament swims faster in a heterogeneous environment of free obstacles (25). (c) *C. elegans* swims faster through a dense field of granular obstacles as it deforms the environment (26). (d) Density map of the shear rate (on a logarithmic scale) near a swimming body in a viscoplastic medium at large Bingham number, showing local fluidization (27). All figures reproduced with permission.

As the obstacles become larger they have an even greater impact on swimming organisms. If they are fixed in space their hydrodynamic reach is roughly independent of size - each appears as a “Stokeslet” singularity in the fluid flow, rather than as a higher-order “stresslet” disturbance field (28). Changes in swimming are even predicted at low obstacle volume fractions. Leshansky showed that the presence of stationary obstacles in the fluid increases the swimming speed and efficiency of a helical filament with a fixed rotation rate or even with fixed power input (**Figure 2b**), essentially by pushing off of the surrounding obstacles (through the fluid) (25, 29). Experiments with *C. elegans* showed too an enhanced mobility in such environments due to an increase in tangential/normal drag anisotropy (**Figure 2c**) (26).

Greater obstacle volume fractions can result in additional complex features. The speed and efficiency of swimming in a viscoplastic fluid, which flows only beyond a critical stress, is characterized by the Bingham number, Bi , a characteristic ratio of the yield and viscous shear stresses. **Figure 2d** shows the density of fluid shear rate $\dot{\gamma}$ on a logarithmic scale near a swimming sheet at large Bingham number. Locomotion is critically dependent upon the fluidization of the environment local to the body surface and may involve the transport of plugged material regions (27, 30).

Type I problems also include systems with a yet broader view of swimming, like the locomotion of sandfish lizards and snakes through dry granular media (31, 32). So long as the relaxation time of the microstructure is small compared to the body’s rate of motion, swimming through fluids with other unusual behavior may still appear as a Type I system.

One such example is swimming in media with a fixed orientational order (e.g. a transversely isotropic fluid, (33–35)). The local order often has a longer relaxation timescale, however, which takes us in the direction of Type II systems.

II. Large De , small Bn , small ϕ : a single swimmer in a suspension of small deformable obstacles

The antibodies lined up side by side, their spaghetti strand projections entangling. (17)

In Type II systems the obstacles express their own relaxation features in a more significant way. They might be long-chain polymers, elastic networks or gels, or molecules which, though individually rigid, slowly relax together into order or to a disordered equilibrium state. Mammalian spermatozoa encounter several such complex fluids, including glycoprotein-based cervical mucus, mucosal epithelium inside the fallopian tubes, and actin-based viscoelastic gel outside the ovum (36, 37). The relaxation may also be diffusive in nature; a dilute suspension of rigid rods may become more aligned by a flow, only returning to a isotropic orientational distribution on a timescale set by the fluid viscosity and temperature.

Shear-dependent viscosity

Shear-dependent viscosity, shear-thinning in particular, appears often when a solvent is host to a suspension of small immersed obstacles or highly deformable polymers. A suspension of elongated particles tends to align with a background shear flow, reducing the bulk viscous resistance. The Carreau number $Cu = \lambda\dot{\gamma}$ is a dimensionless rate of the timescale λ of the environment’s relaxation process and the timescale associated with the local shear rate, $\dot{\gamma}^{-1}$ (38). Mucus, for instance, is significantly shear-thinning - with a relaxation time λ on the order of 1000 s, its viscosity begins to drop at $\dot{\gamma} \approx 10^{-3} \text{ s}^{-1}$, then decreases by four orders of magnitude until $\dot{\gamma} \approx 10^2 \text{ s}^{-1}$ (39, 40). In a swimming system the relevant shear rate is often that generated by the motion of a swimming body, and the Carreau number is precisely the comparison of timescales T_{obs}/T_{swim} in **Figure 1** (i.e. it could as well be called the Deborah number if the flow is oscillatory, or in a constantly sheared fluid the Weissenberg number, introduced below).

Depending on the fluid, swimming in such an environment could instead be classified as a Type I system, as the obstacles themselves need not have an intrinsic deformability or timescale to confer shear-dependent bulk properties. Even in the relatively simple environment composed of a solvent and a suspension of shear aligning rigid rods, Brownian fluctuations introduce a relaxation timescale at the ensemble level. Fluid deformability might in this case be interpreted as the malleability of the distribution of obstacle orientations. A ratio of diffusive relaxation and flow timescales in this setting is generally called a Peclet number, Pe .

Experiments with the workhorse of undulatory locomotion, the nematode *C. elegans*, showed no substantial change in either the body kinematics or swimming speed in a shear-thinning Xanthan gum polymeric solution (41) (**Figure 3a**). In a polystyrene colloidal suspension, however, the stroke form changed and swimming speeds increased by up to 12%, while swimming efficiency continued to increase even once the swimming speed saturated (44). In this second effort it was suggested that the effects were more apparent due to a larger viscosity contrast near the shear rates relevant to the swimming motion.

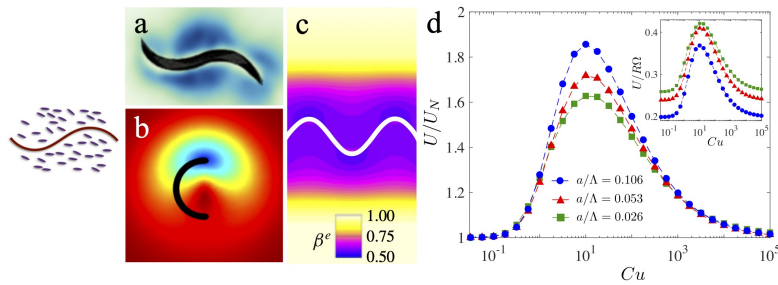


Figure 3

Type II systems: shear-dependent viscosity. (a) Velocity magnitude near a swimming *C. elegans* in a shear-thinning fluid (41). (b) Viscosity field due to the prescribed motion of a helical body in a shear-thinning fluid, resulting in swimming enhancement (42). (c) Similar viscosity stratification near a swimming sheet, also resulting in increased swimming speeds, with Cu the Carreau number and β^e the viscosity relative to the zero shear rate viscosity (43). (d) A Goldilocks zone of Carreau numbers Cu for confinement-like swimming enhancement of helical bodies for a few filament aspect ratios (42). All figures reproduced with permission.

Helical swimmers in a shear-thinning fluid showed even greater speed increases of up to 50% in experiments (45) and beyond in simulations (**Figure 3b**) (42). Similar results were found using model swimming sheets (43). **Figure 3c** shows the viscosity relative to the zero shear rate viscosity at large Carreau number due to the undulatory motion of a swimming sheet with a prescribed motion, showing a very large region of diminished viscosity. Rather than being the result of surface-localized viscosity reduction, it has been suggested that the speed enhancement is due to a confinement-like effect owing to viscosity stratification. The more viscous regions appear as confining walls, apparent in **Figure 3b,c**, revealing a connection between Type II systems and Type III systems (43, 45, 46). The large amplitude body motions used in these numerical studies were also important - the effects of shear-dependent viscosity on the speeds of undulatory model swimmers enters only at fourth-order in the dimensionless amplitude (39).

The swimming speed relative to the Newtonian swimming speed for helical swimming in a shear-thinning fluid is shown in **Figure 3d** as a function of the Carreau number. For both small and large Carreau numbers the environment has a nearly constant viscosity everywhere and the fluid acts as an effective Newtonian fluid. Since the swimming speed of a body in a Newtonian fluid is independent of viscosity for fixed kinematics, the Newtonian swimming speed is recovered at these extremes. In the “Goldilocks zone” of Cu of order 1-10, however, when the relaxation rate is comparable to the rate of body motion, the viscosity change has a more detailed spatial structure and swimming enhancement is observed. Theoretical investigations using the model tangential squirmer, meanwhile, revealed a speed *reduction*, in this range of Carreau numbers (47). The details of how the boundary conditions and the resulting viscosity stratification affects swimming is thus not always easy to guess.

Viscoelasticity

Shear-dependent viscosity is among the simplest non-Newtonian bulk fluid features to consider. Short-range interactions among constituent molecules, or intrinsic relaxation times,

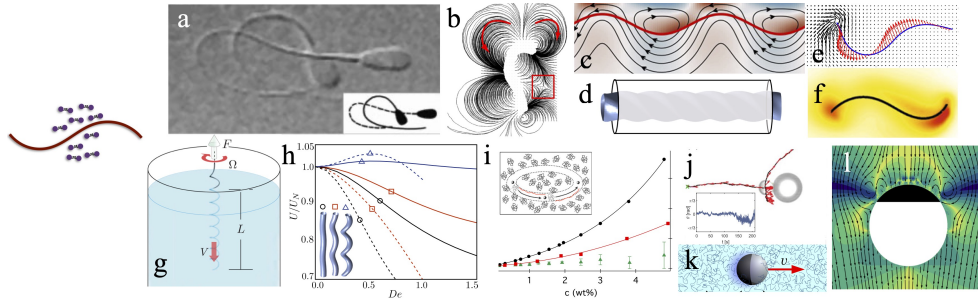


Figure 4

Type II systems: viscoelastic fluids. (a) Spermatozoa become hyperactivated and swim faster (48). (b) The motion of *C. elegans* creates stagnation points in the flow and swims more slowly (49). (c) Streamlines generated by a swimming sheet near a boundary in a viscoelastic fluid (50). (d) Swimming and pumping are modified through the mode-dependent complex viscosity, even in a confined domain (51). (e) Focusing of polymeric stress near the tips of a swimming sheet of fixed gait (52); and (f) with a stress-dependent gait (53). (g) Schematic of an experiment showing enhanced propulsion of helical filaments in viscoelastic fluids (54). (h) Scaled swimming speed across Deborah numbers for three different helical amplitudes, by helical waves (solid lines) and rigid rotation (dashed lines) from simulations (55). (i) Viscosity of a polymeric fluid vs. polymer concentration using a rheometer (circles), microrheology with a large bead (squares) and a flagellum diameter sized bead (triangles), suggesting strong shear-thinning at that scale (inset) (56). Tangential squirmers in viscoelastic fluids: (j) with geometric confinement (57); (k) showing increased rotational diffusivity (58); and (l) driven by autophoresis (59). All figures reproduced with permission.

introduce more dynamic bulk properties. How do such bulk features affect swimming organisms? Unlike in Newtonian fluids energy is temporarily bound into the fluid, which can either aid or resist self-propulsion. Extra fluid stresses can even change the shape of a swimming body or its motility organelles. Flagellar beating by spermatozoa becomes “hyperactivated” in viscoelastic fluids (**Figure 4a**) improving their mobility (60). But viscoelastic environments can reduce swimming speeds as well, as observed in experiments using *C. elegans* (**Figure 4b**) (49); see also the review by Sznitman and Arratia (61).

Such fluids are commonly characterized by the Weissenberg number, $Wi = \lambda \dot{\gamma}$, yet again a product of a relaxation time λ (here an elastic relaxation) and a shear rate $\dot{\gamma}$. In swimming problems, the shear rate is often oscillatory due to the periodic motion of motility organelles like flagella and cilia. Accordingly the Deborah number $De = \lambda \omega$ is more commonly used, where ω is the frequency of oscillation. The subtle distinction between the two depends on yet another length comparison. The magnitude of the shear rate in an oscillatory setting is $\dot{\gamma} = A\omega/L$, with A the oscillation amplitude and L the length scale of the oscillating body, thus $Wi/De = A/L$ which can be small or large in the same fluid. Many more details about Type II systems in particular can be found in recent reviews of swimming in viscoelastic fluids by Elfring and Lauga (62) and Li et al. (63), and of active colloids in complex fluids by Patteson et al. (64).

Viscoelastic model fluids like the Stokes/Oldroyd-B equations (38) have been used to show that speeds should decrease monotonically with the Deborah number for infinite swimming sheets (65, 66) and helical bodies (51, 67, 68) upon the steady propagation of small amplitude waves. For small amplitude perturbations to the fluid, frequency space provides

a natural decomposition of viscous and elastic effects, and explains why the same Deborah number dependence arises for both undulatory and helical motion (62, 69), even in confined systems (**Figure 4c,d**) (50, 51). Mobility enhancement in a purely viscoelastic fluid thus requires large amplitude body motions, finite length, or asymmetric beating, which have been explored numerically with fixed kinematics (52), deformable bodies (53, 66, 70, 71), and mixed wavespeeds (72). **Figure 4e,f** show the added polymeric stress near the tips of finite swimming sheets for fixed kinematics and for a deformable swimmer. These additional stresses can either aid or restrict propulsion depending on the nature of the stroke (52, 53). A spatially increasing wave amplitude introduces a flapping-like motion which would not generate a net thrust in a Newtonian fluid owing to kinematic reversibility, but does in a viscoelastic fluid, leading to swimming enhancement (73). Near walls, the fluid pinned between the swimmer and a surface can experience large local strains and stresses which in turn can have an outsized effect (66, 74). Similarly, such large strains near the body might be created by swirling flows, either by the body or by rotating flagella; the associated hoop stresses so generated can also provide a boost to swimming speeds (75, 76).

Pathogen mobility in complex fluids is another area of interest for unobvious reasons. Helical *Leptospira* and *B. burgdorferi* cells, the root cause of Weil's and Lyme diseases, respectively, swim faster in viscoelastic environments (77, 78). Experiments using a Boger fluid (54) and numerical solution of the Stokes/Oldroyd-B equations (55) recovered such enhancements at large helical amplitudes (**Figure 4g**). **Figure 4h** shows the swimming speed relative to the Newtonian swimming speed for helical bodies of different helical amplitudes across a range of Deborah numbers, with values over one achieved only beyond a critical large amplitude for both helical waves (solid lines) and rigid body rotation (dashed lines) (55).

But relating experiments to simulations and theory can be complicated by the fact that shear-thinning and viscoelasticity often occur together in real fluids and can depend on distinct features acting simultaneously on multiple-scales (46, 56). **Figure 4i** shows the viscosity of a polymeric fluid as a function of polymer concentration using a rheometer (circles), microrheology with a 980 nm bead (squares) and microrheology using a small bead closer to the size of a flagellar cross-section (40 nm, triangles) showing no appreciable dependence on polymer concentration. On the scale of the flagellum, then, the resistance is merely due to the solvent viscosity, which was proposed as being due to severe shear-thinning in the region near the flagellum (inset) (56, 79). The fixed geometry of model tangential squirmers offers additional theoretical insight on the role of viscoelasticity, from the dependence on stroke asymmetry and geometric confinement (**Figure 4j**) (57, 74), to changes in rotational diffusivity and strong dependence on external forcing (**Figure 4k**) (58), and how autophoretic motion couples to the complex generated flow (**Figure 4l**) (59). Novel methods and devices for swimming body rheometry continue to be developed, with a particular focus on future medical applications (80–82). We refer the reader to the particularly germane review by Venugopalan et al. (83).

Networks and gels

Rather than moving freely, the obstacles may instead be connected to each other. In this case the relevant relaxation timescale(s) may be that of a porous or cross-linked network of fibers or a gel. **Figure 5a** shows a spermatozoan swimming through the elongated glycoproteic meshwork in cervical mucus, showing that the obstacle size is much closer to

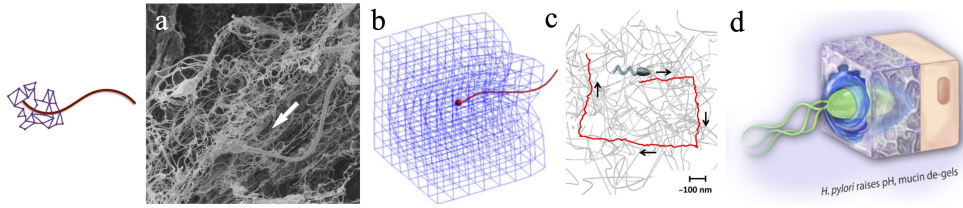


Figure 5

Type II systems: networks and gels. (a) Spermatozoa swim through the anisotropic glycoprotein meshwork in cervical mucus (84). (b) Enhanced swimming of an undulating body through a stiff elastic network (85). (c) A magnetically-driven synthetic swimmer probes a gel (86). (d) *H. pylori* chemically alters the rheology of its environment, improving its mobility (87). All figures reproduced with permission.

the swimmer size than is often appreciated. Using the pore size as an obstacle length scale, for microorganisms swimming through mucus the Benes number B_n can be in the range $0.1 - 2$ (88). Similar to the example of shear-thinning by a moving flagellum suggested by **Figure 4i**, continuum theories using two-phase fluid models suggest that the nature of the network (and so the boundary conditions) on the swimming body are of critical importance for both swimming speed and efficiency (89, 90). Enhanced motion has been found for undulatory swimmers moving through stiff networks and for magnetically-driven helical bodies swimmers through gels whose meshsize is roughly the same size as the swimmer (86) (**Figure 5b,c**). Some organisms even alter the physics of their environment through chemical processes which improve mobility. Urease enzyme released by the pathogen *H. pylori* modulates the fluid's local pH but also reduces mucin viscoelasticity, allowing the bacteria to penetrate a mucus lining protecting the gut (87) (**Figure 5d**).

Anisotropic fluids

Our last example of a Type II system is swimming in an anisotropic medium which relaxes towards orientational order. Network-formation in mucus can lead to such liquid-crystalline order (91), and may be relevant to spermatozoa navigation through the cervical canal (**Figure 5a**) (84). A model fluid used to investigate such environments, both experimentally and theoretically, is a liquid crystal. The standard models and fluids used, like the bacteria-friendly lyotropic chromonic disodium cromoglycate (DSCG), are composed of symmetric rodlike molecules, resulting in ordered nematic phases upon cooling, and randomly oriented isotropic phases above a critical temperature. Near the phase transition the motion of a *B. subtilis* cell through the environment can temporarily melt the liquid crystal, leaving an alluring helical trail in its flagellar wake (**Figure 6a**) (92).

The details of swimming in a liquid crystal can depend strongly on another feature not present in many other complex fluids, a surface anchoring energy, which penalizes departures from a given molecular orientation there due to surface chemistry. The continuum director field describing the orientation of (stacked) DSCG molecules, for example, preferentially anchors to biological membranes in the tangent plane (93). As a consequence, when elongated bacteria are placed in such fluids they tend to align with the local director field - the elastic energy in the bulk liquid crystal is smaller when the body is more "streamlined". Exploiting this observation, director-guided motion is seen along the surface of nematic tac-

toids (**Figure 6b**) (93) and has been used to trace a long path for cargo-carrying *Proteus mirabilis* cells to follow (94) (**Figure 6c,d**). Liquid crystal director fields are also bound by topological constraints, which generically result in the presence of defects, points at which the director field is non-differentiable (95). Different defects induce different bacterial behavior; $+1/2$ defects encourage accumulation while $-1/2$ defects (**Figure 6e**) result in mean depletion (96, 97).

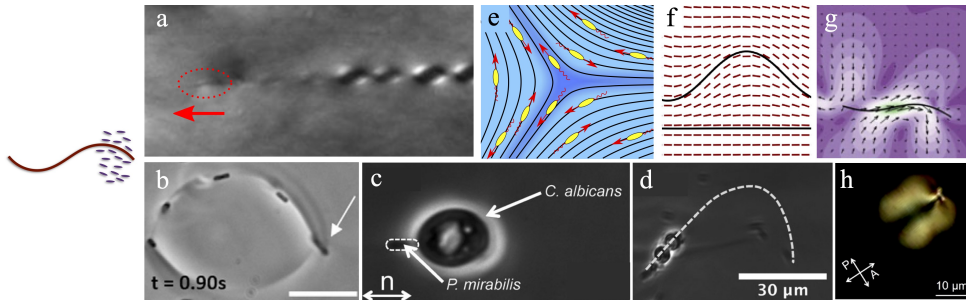


Figure 6

Type II systems: anisotropic fluids. (a) Nematic-biphasic melting in the wake of a swimming *B. subtilis* cell (92). *Proteus mirabilis* in director-guided motion (b) near a nematic tactoid (93) and pushing (c) a large yeast cell and (d) two microbeads along prescribed paths (94). (e) Depletion of bacteria near a $-1/2$ topological defect (97). (f) Director field near a waving sheet and an infinite wall in a liquid crystal with strong tangential anchoring conditions (98), and (g) around a finite body, with velocity field (and magnitude, colored) (99). (h) A self-propelling liquid-crystal droplet swims through a bulk nematic phase (100). All figures reproduced with permission.

Theoretical perspectives on swimming in anisotropic fluids are once again stymied by a dramatic coupling of nonlinearities and an avalanche of dimensionless groups, but asymptotic analysis in some simplified settings has provided some insight. The predictions which have emerged are surprising, for instance an infinite swimming sheet can swim either with or against the direction of its wave propagation. The direction depends on the rotational viscosity, which determines the rate at which the fluid's orientational order is recovered, and thus the rate at which an elastically generated “backflow” is produced (33, 98). As in the case of isotropic viscoelastic fluids, the bulk elasticity can play the role of effective confinement leading to increased swimming speeds. The degree to which the director field may be deformed is characterized by the Ericksen number $Er = \mu UL/K$, a ratio of the viscous to elastic forces in a flow, where μ is the fluid viscosity, U and L are characteristic velocity and length scales, and K is a bulk elastic modulus (a Frank elastic constant) (95). Here again, choosing $T_{obs} = \mu L^2/K$ as an elastic relaxation timescale, and $T_{swim} = L/U$ a swimming timescale, the Ericksen number $Er = T_{obs}/T_{swim}$ is the Weissenberg number in different clothing (or the Deborah number in the oscillatory setting).

The constituents of a liquid crystal generally have a preferred orientation on a given surface, and a surface anchoring energy represents the cost of deviation from this configuration there - large anchoring strengths can distort the field well into the bulk (95). **Figure 6f** shows the director field of a nematic liquid crystal around an infinite sheet swimming near a flat surface at small Ericksen number, with strong tangential anchoring on both boundaries. While the rotational viscosity and backflow can alter the swimming direction, its effects are substantially magnified when the anchoring strength is large (98). Simulations

of finite-length swimming sheets show similar results but also reveal that the director field deformations and associated elastic stresses, like for swimmers in viscoelastic fluids, are largest near the tail (**Figure 6g**) (99).

Our last example blurs the lines between Type II and Type IV systems. A liquid crystal droplet can swim through a bulk nematic phase due to initial symmetry breaking by Marangoni stresses on the surface, with coherent motion supported by orientation-dependent van der Waals forces at the boundary (**Figure 6h**) (100). As is generally the case for swimming in anisotropic environments, the swimming direction is biased into the direction of the background director field.

III. Small De , large Bn , small ϕ : a single swimmer near a large rigid obstacle

There was a soggy collision of a bacterial rod with the ship. The substance of the bacterium bent about the curve of the window, sprang back into shape and bounced off, leaving a smear that washed off slowly. (17)

Type III represents systems with a single swimmer in a Newtonian fluid near a rigid obstacle. Depending on the Benes number the obstacle geometry may come into view. Many features of swimming near obstacles, however, is informed by the limit of infinite Benes number (e.g. swimming near an infinite wall).

Swimming near a wall

For very large Benes number the obstacle may appear to the swimmer as a flat wall. One early theoretical study by Katz placed Taylor’s infinite swimming sheet model with fixed gait near a rigid boundary (101). The swimming speed was found to increase dramatically as the body neared the wall but with greater energetic cost. This fact has been used to rationalize swimming enhancement when complex fluid stresses produce effective confinement, as we have already seen in some Type II systems.

More complex body dynamics and trajectories also appear when a boundary is nearby, including surface accumulation (114) and circular orbits (**Figure 7a,b**) (103, 115–117). *Chlamydomonas* algae cells scatter from a wall at an angle determined by their flagellar geometry (**Figure 7c**) (104, 118), and the random “tumbling” of *E. coli* is suppressed near surfaces due to increased hydrodynamic resistance (119, 120). Hydrodynamic effects can be substantial, metallic synthetic swimmers can even swim upwards against gravity using the hydrodynamic interaction with a wall (**Figure 7d**) (105). Surface accumulation may also be a statement of mean behavior, with individual swimmers undergoing periodic departure and return (110, 121).

Modeling and simulation has been used to better understand the extent to which hydrodynamics alone can describe these phenomena. Far-field hydrodynamics capture many features robustly. The model Janus swimmer in **Figure 7e** was used to explore the accuracy of such theories, showing them to be remarkably accurate down even to swimmer-wall distances well below the swimmer length (106, 122). But to understand the interplay between flagellar beating and surface interactions requires more detailed flagellum-resolving simulations like those shown in **Figure 7f,g** (107, 108, 123–126). The combination of wall effects and a background flow can encourage an unexpected upstream swimming due to a “weathervane” effect (**Figure 7h**) (109, 127–129). Body geometry and fluctuations can also strongly affect orientational statistics (125, 130–132), as elegantly explored in configuration

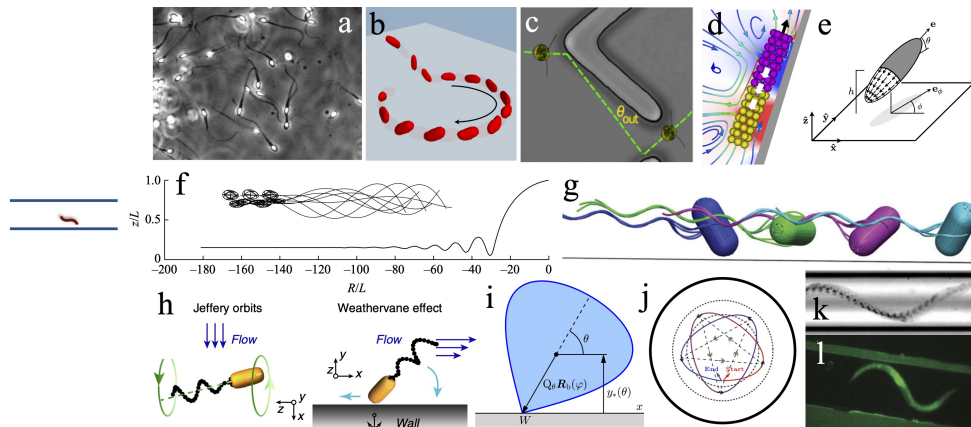


Figure 7

Type III systems: swimming near a wall. (a) Surface accumulation of spermatozoa (102). (b) Holographic recovery of circular swimming of an *E. coli* cell (103). (c) A *Chlamydomonas* cell departs from a wall at an angle related to its flagellar geometry (104). (d) Swimming up a wall against gravity (105). (e) Far-field models are often adequately predictive (106), but more detailed simulations can resolve the role of cell shape and deforming bodies, for (f) dynamic accumulation of spermatozoan swimming (107) and (g) wobbling of multi-flagellated cells (108). (h) A “weathervane effect” due to a background flow can result in upstream swimming (109). (i) Body shape can strongly affect near-wall scattering and statistics (110). (j) Confinement-induced periodic trajectories of a model swimmer (111). (k) A confined *Paramecium* cell swims with a helical trajectory (112). (l) *C. elegans* combines swimming and crawling motions under confinement (113). All figures reproduced with permission.

space by Chen & Thiffeault with the asymmetric model swimmers shown in **Figure 7i** (110). Other alluring trajectories abound including periodic dynamics under confinement of model swimmers (**Figure 7j**) (111, 133–136) and in experiments with a *Paramecium* cell (**Figure 7k**) (112).

Helical bodies in cylindrical confinement enjoy a similar speed enhancement as that described by Katz, though the details depend on the helical geometry and distance to the boundary (51, 137). The optimal pitch angle for self-propulsion is similarly affected. The compliance of the cell and particularly any thin, highly deformable motility organelles can thus strongly affect both swimming speeds and energetic costs (138). Larger slender bodies like *C. elegans* also deform under confinement (**Figure 7l**), and their motility is affected accordingly (113, 139).

Geometric obstacles

As the Benes number decreases the obstacle shape begins to come into view ($Bn = O(1)$ when the body and obstacle are roughly the same size). Billiard-like motion, intermittent periods of entrapped orbiting states, and randomized escape behavior are observed in a fluid with finite-sized obstacles in both synthetic and living systems (**Figure 8a,b**) (140, 141). The far-field flow generated by a non-Brownian pusher-type swimmer (a dipolar swimmer that expels fluid along its swimming direction and draws it in laterally) near a spherical obstacle suggests hydrodynamic entrapment above a critical Benes number which depends

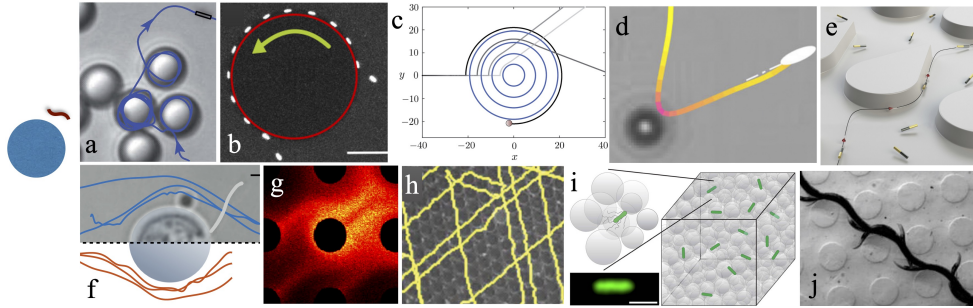


Figure 8

Type III systems: geometric obstacles. (a) Scattering and entrapment of synthetic swimmers by spherical colloids (140); and (b) of *E. coli* cells by cylindrical posts (141). (c) Trajectories of pusher-type swimmers around colloids of four different sizes. Scattering is non-monotonic in the colloid size, while entrapment is predicted above a critical Benes number (e.g. colloid size) which depends on the dipole strength and swimmer diffusivity (142). (d) Cell transport may be enhanced due to scattering events even at low obstacle density (143). (e) Scattering may be guided by obstacle shape (144). (f) Entrainment of small obstacles depends on their size and the mechanism of propulsion (145). (g) A simulated cloud of non-interacting swimmers spreading through a periodic array of posts (146). (h) Repeated surface interactions in porous media can focus swimming trajectories (147); or (i) result in effective diffusion (148). (j) *C. elegans* transitions from swimming to crawling in a structured environment to enhance mobility (149). All figures reproduced with permission.

on the dipole strength. **Figure 8c** shows the trajectories of pushers swimming towards colloids of radius 5, 10, 15, and 20 times the body size, showing a non-monotonic scattering angle with increasing colloid size and hydrodynamic entrapment by the largest obstacle (142). With the inclusion of thermal fluctuations, trapping time statistics depend most notably on the rotational diffusivity of the swimmer. A puller-type swimmer (which instead draws fluid inward along its swimming direction and expels it laterally) can pull itself into an entrapped state near much smaller obstacles.

If entrapment does not occur or is only temporary, the interaction can still affect the long-time statistics. Such scattering events can enhance transport even at low obstacle densities (**Figure 8d**) (143). The mechanism of self-propulsion (142, 150–153) and obstacle shape (144, 154), for instance the teardrop-shaped obstacles shown in **Figure 8e**, can also strongly affect the interaction with and departure from the surface. Sorting and rectification devices meant to exploit such interactions have been constructed and explored, including funnels and gears (16).

For smaller obstacles it becomes more important whether or not they are fixed in space or free to become entrained by a passing swimmer. If entrained, the shape and stroke of the swimmer become particularly important (**Figure 8f**) (145, 155). Transport of yet smaller obstacles, or even fluid particles, return us closer to Type I problems and the general question of fluid entrainment by swimming bodies (156). A direct exploration of the Benes-number dependence on entrapment and particle entrainment is found in Ref. (157), and a generic enhancement of swimming by the reduction of wobbling in colloidal suspensions is described in Ref. (158).

There may instead be many large obstacles to navigate, and the dynamics described

above may take place over repeated interactions. **Figure 8g** shows a simulated cloud of active Brownian swimmers spreading in a periodic array of posts. Generic features in such systems include boundary layers and thin regions of increased swimmer concentration in the “wake” of an obstacle (146). In systems with more tightly packed obstacles, synthetic swimming particles can hop from colloid to colloid with a trapping time that depends on fuel concentration, while *E. coli* trajectories are rectified into long, straight runs (**Figure 8h**) (147). The uncertainty in trapping times and exit orientations leaving one obstacle leads to an effective diffusion through a bulk porous medium (**Figure 8i**) (148). In this example, depending on whether the obstacle size is chosen to be the size of the colloid, roughly $10\mu\text{m}$, or the narrow pore size between obstacles, $10^{-1}\mu\text{m}$, the Péclet number ranges from 10^{-2} to 1.

As usual body deformability can be important; *C. elegans* for instance transitions from swimming to crawling motions to enhance its mobility in a structured environment. **Figure 8j** shows this nematode traversing a periodic array of obstacles. When Bn is order 1, particularly if the undulatory wavelength is the same size as the obstacles, the swimming is focused into straight trajectories like the *E. coli* cells in **Figure 8h** as the body pushes off each obstacle one after another (149, 159).

IV. Large De , large Bn , small ϕ : a single swimmer near a deformable obstacle

The white cell was tremendous. It was five times as large in diameter as the Proteus, perhaps larger; a mountain of milky, skinless, pulsing protoplasm in comparison to the individuals watching. (17)

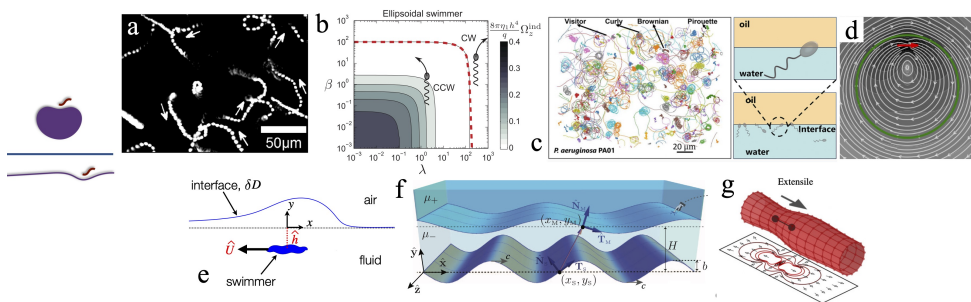


Figure 9

Type IV systems. (a) Counter-clockwise circular trajectories of *C. crescentus* cells at an air-water interface (160). (b) Purely hydrodynamic arguments show similar counter-clockwise (CCW, free surface) to clockwise (CW, solid wall) rotations depending on the viscosity ratio λ and the surface viscosity β (contours of the rotation rate are shown) (161). (c) Free and adhered states of *P. aeruginosa* cells at an oil-water interface - distinct trajectories (left) are due to differing trapped states (right) (162). (d) Flows in and along the surface of a confining droplet due to an interior point force (163). (e) Normal surface deformations may be generated by distant swimmers (164). (f) Closer swimmers can deform an interface more substantially, resulting in stronger speed and efficiency adjustments (165). (g) Soft confinement can either increase or decrease the speed of model swimmers (166). All figures reproduced with permission.

In Type IV systems a large obstruction relaxes on a timescale longer than or commensurate with that of a single organism’s motion. Examples include air-water interfaces,

oil-water interfaces (167), thin films (168), and mucus-lined tissues like those found in the mammalian reproductive tract (36). Even if the action of a swimmer is insufficient to drive substantial normal surface deformations, the freedom of tangential interface motion can affect swimming behaviors. For example, the orientation of the circular swimming patterns of organisms like *E. coli* are reversed relative to what is observed for swimming near a rigid wall (**Figure 9a**) (160, 161, 169, 170). This change in observed behavior can be rationalized by examining the hydrodynamics of swimming with a mirror image across the interface (**Figure 9b**) (106, 161, 169, 171, 172). But the behavior can also be very sensitive to the surface adsorption of organic materials and surfactants, which can render the surface more or less rigid (160).

Surface absorption of the swimmer is possible as well, which can lead to distinct trajectories depending on the nature of the trapped state. **Figure 9c** shows numerous trajectories of *P. aeruginosa* cells at an oil-water interface, which include diffusive paths, curved trajectories, and rapid “pirouette” rotations (162). The tangential flows and resultant swimmer dynamics generally depend on the relative obstacle size or interfacial confinement and the common possibility that surfactants are present on the interface (**Figure 9d**) (163, 173). Surfactants can rigidify the interface and nudge the system back towards Type III interactions of a swimmer with a rigid obstacle or wall (174, 175).

Stronger swimmers, or softer boundaries, can result in normal surface deformations as well. Many theoretical techniques have been used to probe this problem including far-field approximations (**Figure 9e**) (176), a conformal mapping approach (164), and small amplitude asymptotic analysis for swimming sheets (**Figure 9f**) (165) and squirmers (177). Depending on the nature of the swimmer and the surface physics, the deformability of the boundary can result in either enhancement or retardation of swimming speeds for a given swimming kinematics (**Figure 9g**) (165, 166). Even tighter confinement can lead to even more dramatic boundary and swimmer shape deformations. A model amoeboid swimming through a narrow compliant channel, for instance, undergoes a marked decrease in swimming speeds as the channel narrows (178, 179).

V. Small De , small Bn , large ϕ : many swimmers in a suspension of small rigid obstacles

Type V systems feature environments with small rigid obstacles, as in Type I, but with a sufficiently large swimmer concentration ϕ so that their interactions become relevant. With Bn small the fluid is again reasonably approximated as a continuum medium at the scale of the swimmers. A first step in the direction of understanding large swimmer concentrations is to consider the interactions of two swimmers. When two swimmers approach each other the details of their shapes and swimming cycles come into view. For example, waving sheets and filaments can be synchronized through hydrodynamic interactions - **Figure 10a** shows two nearby swimming spermatozoa swimming in synchrony (180). But hydrodynamic interactions are not always dominant in such settings. The synchronization of *C. elegans* nematodes, for instance, is based more on the effects of steric hindrance (**Figure 10b,c**) (181).

The collective dynamics of many swimmers, meanwhile, remains a particularly vibrant research area which has been treated to excellent and deeper treatments beyond the scope of this review (4, 189–196). Among the main features observed in these systems, the long-range nature of hydrodynamic interactions in viscous fluids can result in positional and

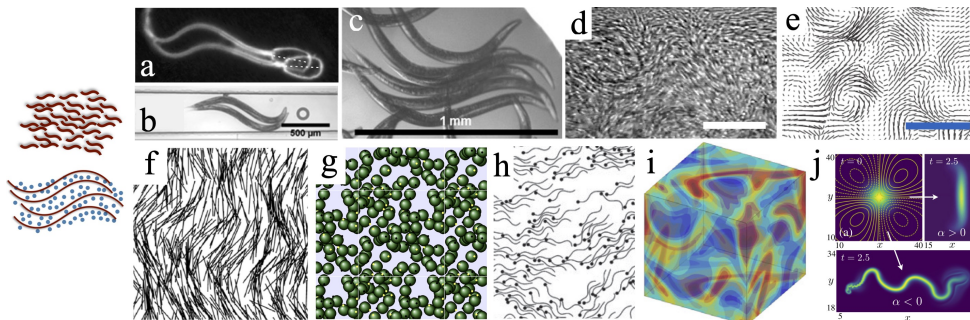


Figure 10

Type V systems. (a) Synchronization of swimming spermatozoa (180); (b,c) and *C. elegans* (181). (d) Collective motion of *B. subtilis* cells shows correlations on much larger scales than the individual swimmer size (scale bar is $35\mu\text{m}$) (182). (e) Velocity field from collective simulations resolving individual swimmers (scale bar is 5 swimmer lengths) (183). (f) Onset of an orientational instability in a suspension of nearly aligned “pusher” swimmers (184). (g) Collective motion of model spherical squirmers (185). (h) Synchronization and aggregation within large groups of model spermatozoa (186). (i) Swimmer concentration field via solution of moment equations in a coarse-grained theory (187). (j) Self-stretching of a Gaussian concentration of rightward-pointing swimmers, along the swimming direction and unstable for pushers ($\alpha < 0$) or transverse to the swimming direction for pullers ($\alpha > 0$) (188). All figures reproduced with permission.

orientational correlations among groups of swimmers even at volume fractions as low as $\phi = 1-2\%$ (182, 197). Such correlations can depend on body shape - rotation and alignment is different for sphere-like and rod-like bodies (28). At large swimmer concentrations, new complex phenomena begin to emerge. Swimmer interactions can lead to increases in effective velocity and diffusion. For example, **Figure 10d** shows a suspension of *B. subtilis* cells, each roughly $4\mu\text{m}$ long, with structures observed on the larger scale of the $35\mu\text{m}$ bar on the bottom right (182). These structures lead to enhanced diffusion of tracer particles that depend on their size (198) and shape (199). Interactions among externally driven rotating bodies can result in clustering, colony-scale rotations, and so-called odd viscosity (196, 200, 201). Such dynamics have also been observed in swimming suspensions of *T. majus* bacteria cells (202) and starfish embryos (203).

Simulations and theoretical advances

A number of agent-based simulations have been used to explore the mechanisms causing the group behavior. Hernandez-Ortiz et al. (183) showed that the type of swimming (either pushed from the back or pulled from the front) changes the hydrodynamic interactions and thereby the large scale group behavior. As in experiments, the velocity field shown in **Figure 10e** shows correlated motion on a scale much larger than the individual swimmer size; the included scale bar is 5 swimmers long. A generic feature in active suspensions for small ϕ is the emergence of long-range orientational order for pusher-type swimmers, seen for instance in simulations of many pusher-type swimming rods (**Figure 10f**) (184). Such group behavior is found in simulations using spherical squirmers as well (**Figure 10g**) (185). In this system at higher swimmer concentrations the isotropic state destabilizes and relaxes into polar order for both pushers and pullers, unlike in dilute theories for which only

isotropic suspensions of pushers are orientationally unstable.

These agent-based simulation models have quantified how hydrodynamic interactions and swimmer shape impact swimmer velocity and orientational correlations (184, 204–208). They have also used passive tracer particles which are advected and mixed by the flows created by the swimmers as a method to quantify collective behavior (209–211). Within large groups, clustering is observed, and is attributed to steric and hydrodynamic pairwise interactions similar to those seen in dilute suspensions (**Figure 10h**) (186). Such results highlight one feature that is currently less understood: how the details of swimmer shapes and their swimming strokes affects short range correlations within systems that show large scale group dynamics (212, 213).

Theoretical advances have involved the derivation and analysis of continuum field equations for the coarse-grained system dynamics (193). Further simplification is found through closure approximations, generating coupled equations for the first few local orientational moments, which produce results similar to those found in full agent-based simulations. **Figure 10i** shows spatial variations in a concentration of pushers which have emerged out of an isotropic state using the Saintillan-Shelley model equations (187). The self-stretching of localized colonies, and a cascade of transverse instabilities in thin concentration bands, provides insight on these more fully developed global dynamics (**Figure 10j**) (188, 214). Recently, field theories that include fluctuations and correlations have been developed to examine the onset of collective behavior (211, 215, 216).

Complex rheology

The activity and orientational order which emerges in these systems can confer the solvent-suspension system with features normally associated with bulk complex fluids. The effective viscosity of fluid containing puller-type swimmers, specifically *Chlamydomonas Reinhardtii*, has been found to increase on account of their swimming activity (217, 218). Suspensions of pusher-type swimmers like *B. subtilis* (14) and *E. coli* (219–221), meanwhile, are found to decrease the effective viscosity of the medium. These generic effects of extensile (pusher) and contractile (puller) suspensions are also recovered theoretically (11, 222). As the swimmer volume fraction increases the decreased viscosity for suspensions of pusher-type swimmers can reach zero, effectively a superfluid state, where the medium can be sheared with no stress, and then into negative effective viscosity, where work must in fact be done to keep the medium from shearing itself (11–15). The superfluid response can also cause shear-banding in the velocity profile (223).

These suspensions are often found to have a swimmer contribution that decreases with background shear rate, as the active stresses which they produce become drowned out by the large scale motion. Many models have computed the contribution to rheological properties from the hydrodynamic disturbance caused by the swimmers. These models show a decrease due to shear-induced swimmer alignment, much like the shear-thinning found in suspensions of passive rods. There is also a diffusive contribution, which can lead to non-Newtonian behavior of the suspension (224).

Suspensions of spherical squirmers have been used to explore the rheology of very high swimmer concentrations, where the lubricating region between individual swimmers dominates their interactions. The effective shear viscosity is found to increase for both pushers and pullers compared to a similar suspension of inert spheres. But for bottom-heavy squirmers the distinction between pushers and pullers returns, and viscosity reductions down to

superfluidity appear again for pusher suspensions (225).

The role of body deformability on active suspensions and their effective rheology remains a generically open area of inquiry, but simulations have revealed that the sign of the effective medium's second normal stress differences depends on body stiffness (226). Other non-Newtonian features due to active suspensions like viscoelasticity (11, 222, 227, 228), and yield-stress behavior (229, 230) have also been predicted. The influence of surfaces described in Type III can also impact measurements of rheological properties (231). For a more detailed analysis of active suspension rheology in general see the recent review by Saintillan (15).

Type V systems include another fairly unexplored territory, active suspensions in media with somewhat larger obstacles (though still smaller than the swimmer size). If those small stiff obstacles are free to move, they may simply alter the viscosity of the suspending fluid. But if the obstacles are fixed either through connections to each other or to the surroundings, they will alter the swimmer behavior in a different way. The stiff connection allows for the dissipation of momentum and the obstacles will generically screen long-ranged hydrodynamic interactions. Instead, short ranged interactions can lead to large scale patterns (232).

$\forall \mathcal{I}$. Large De , small Bn , large ϕ : many swimmers in a suspension of small deformable obstacles

“If you damaged it, chemicals were released into the blood-stream; chemicals that attracted white cells from all the neighboring regions.” “Then, for God’s sake, swim!” (17)

Type II systems were characterized by small obstacles with intrinsic timescales longer than or commensurate with that of a single swimming body. If there are instead many interacting swimmers in such an environment we find ourselves in a Type VI system. The group of swimmers may be invading a shear-thinning viscoelastic solution or gel, or an anisotropic medium like mucus.

Depending on the system, the non-Newtonian bulk fluid features may have a bearing primarily on localized behaviors and interactions, or may reveal structures on much longer length scales than the swimmers themselves. The motion of each swimmer can be changed, as previously described in Type II, and in some settings these changes to individual swimming behaviors might be sufficient for understanding the effect of viscoelasticity on group behavior. But the hydrodynamic interactions may also be modified to produce a group behavior that is not simply a shift or rescaling of theories based on Newtonian fluids.

As the volume fraction of swimmers ϕ increases, the first deviation from individual swimmer dynamics occurs due to pair interactions. Viscoelastic fluids lead to enhanced clustering and synchronization in experiments with spermatozoa (**Figure 11a**). Infinite swimming sheets synchronize in polymeric fluids much more rapidly than they do in a Newtonian fluid (**Figure 11b**) (113, 239). Liquid crystals also alter the strength and anisotropy of pair interactions, which can result in the convergence of swimming speeds (**Figure 11c**) (234). The interaction may depend strongly on surface anchoring conditions on the swimmers and on nearby boundaries. In some cases the liquid crystal can contribute to swimmer repulsion; in others, collisions and group swimming have been observed (**Figure 11d**) (235).

For larger swimmer volume fractions, group behavior on length scales much larger than the individual swimmer size once again emerges as in Type V systems. Changes in the

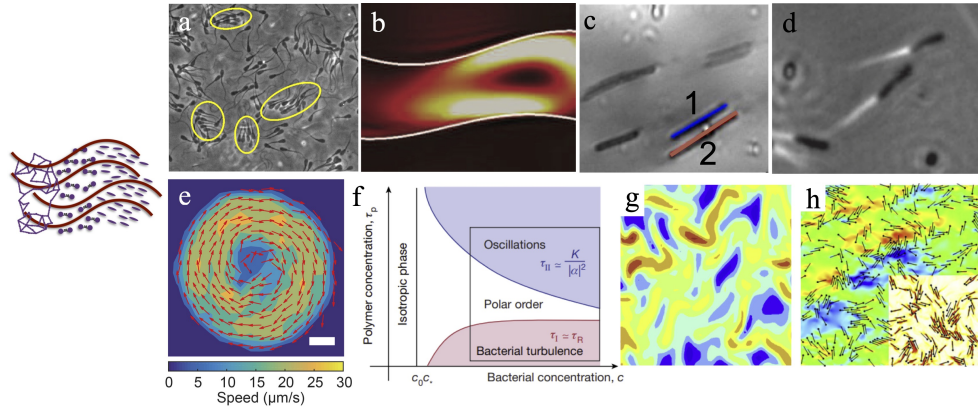


Figure 11

Type VI systems. Interacting swimmers in a fluid with bulk complex features. (a) Viscoelasticity-enhanced synchronization in spermatozoa (233); (b) and in simulations of swimming sheets (113). (c) Swimming speeds of nearby *B. subtilis* cells converge in an anisotropic medium (234). (d) Surface anchoring induces bacterial collision and group swimming (235). (e) Velocity field and magnitude of an active suspension of *E. coli* cells in a viscoelastic medium; and (f) associated phase diagram of ordered and disordered states, including direction-reversing oscillations above a critical polymer concentration (236). (g) Swimmer concentration from mean-field simulations of an active suspension in a viscoelastic medium reveal a reduction of large-scale structures (237). (h) Agent-based simulations show a similar reduction of large-scale structures (238). All figures reproduced with permission.

velocities within large groups have been observed experimentally. **Figure 11e,f** show the instantaneous velocity field of a suspension of *E. coli* in a viscoelastic medium, and a phase diagram of ordered and disordered states across different bacterial and polymer concentrations. For sufficiently large polymer concentration a bizarre effect is observed, the onset of occasional group transport direction reversal (236). Inhibition of large scale group behavior and an increase in swirling oscillations are attributed to a interaction between the time scale of the collective vortex flow and the time scale of elastic fluid relaxation. This example sits at the interface between Type VI and, say, Type VII, as the system behavior depends upon both confinement and bulk rheology, e.g. upon multiple obstacles on multiple scales. The question of classification in any system requires identification of the dominant contribution for the features of interest.

The earliest works to examine these effects theoretically used a continuum field theory to track the dynamics of the active particles and a continuum stress field to track the dynamics of the complex fluid (**Figure 11g**) (237, 240, 241). A prototypical view of group behavior among pushers is as a competition between hydrodynamic interactions that lead to alignment of swimmers and noise that tries to randomize swimming directions. Because the viscous response is driving an instability to group behavior, if the fluid does not fully relax during the instability, a viscoelastic fluid produces less group behavior than a Newtonian fluid with the same zero-shear viscosity. However, because the suspended soft obstacles do contribute to the viscous response, there can be more group behavior than if the obstacles were not present.

In addition to changing fluid instabilities, viscoelastic fluids can change the nature of

group behavior. This group behavior is often characterized by chaotic swirling flows. Viscoelastic stresses can break up these large swirls. This leads to intermittancy similar to turbulent drag reduction; a random isotropic suspension can be unstable, leading to large-scale flows which excite viscoelastic stresses - stresses which proceed to suppress the large-scale flows. Other works modeling group behavior in viscoelastic fluids have tracked interacting swimmers within a continuum viscoelastic fluid (**Figure 11h**) (242). Such models also show a suppression of large scale group behavior and fluctuations in viscoelastic fluids. Alternatively, in liquid crystals with homeotropic anchoring, distortions of the director can mediate swimmer interactions and cause collective effects (235).

Some soft systems do not fully relax at long times due to cross-linking of polymers, as in a gel. These properties have the potential to alter the behavior of concentrated groups. For example, mucus gels can change the swimming and aggregation of bacteria (243). One important feature of such systems is that the swimmers can change their behavior in response to the mechanical properties as well as chemical makeup of the suspending material (244).

VII. Small De , large Bn , large ϕ : many swimmers near a large rigid obstacle

“They won’t bother us, I hope. Any bacteria in the circulatory system reaches a lymph node eventually. It can’t negotiate the narrow twisting channels...”. “Can we?” (17)

The collective dynamics of swimming organisms can be strongly influenced by confinement, which brings us to Type VII systems. Swimming bodies at a surface are more restricted in the orientations that they may exhibit, as seen in Type III systems with single swimmers. At the group level such restrictions can propagate into and influence the bulk suspension organization. For example, suspensions of confined bacteria can settle into a large-scale group rotation (**Figure 12a**) (245). When multiple rotating domains are connected by channels, the direction of bulk flow which is normally selected with equal probability may start to become influenced by neighboring domains, resulting in the possibility of ferromagnetic or antiferromagnetic global states (246). But the relationship between individual body motion and the motion of the group is not always simple. The flagellar motion of cells swimming near the boundary in **Figure 12b** generates a flow in the opposite direction in the bulk, so confinement simultaneously produces both upstream and downstream bacterial transport (247).

Just as in Type V systems, coarse-grained modeling has identified relationships between the geometry of confinement and the strength of the far-field hydrodynamic signal (dipole strength). The interplay between them can result in coherent rotational motion, or deterioration into other classical aperiodic roiling states, or dynamic modes combining features of both (**Figure 12c**) (193, 248, 253). Directed motion is found when the channel width is close to the length-scale of rotating domains in the unbounded system (247). With even tighter confinement, phase transitions to jammed states have been found, explored using suspensions of model spherical squirmers (254).

A boundary may encourage more localized collective behavior as well. Suspensions of spermatozoa near a wall, for example, settle into an array of swimming vortices (**Figure 12d**) (249). But while confinement can encourage the emergence or selection of collective behavior, the screening of flows by nearby boundaries can also inhibit the onset of large scale structures. This was shown numerically in Ref. (255) using a suspension of model swimmers composed of dipolar pushing beads. Screening effects may be partially

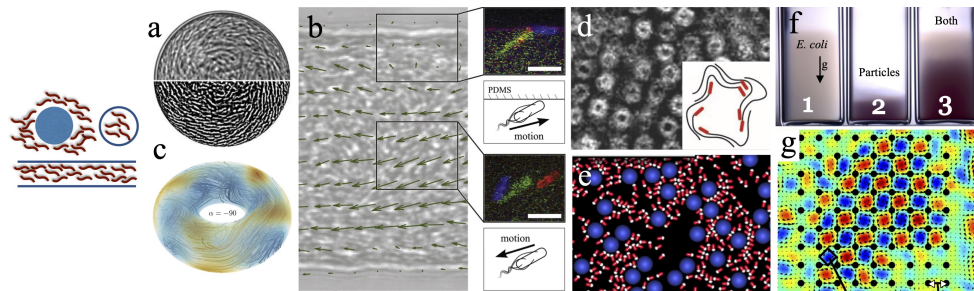


Figure 12

Type VII systems. (a) Edge rotation and bulk counter-rotation due to confinement in a circular domain (245); (b) and in a racetrack, where swimmers in the bulk are carried opposite their orientation by a flow generated by swimmers at the boundary (247). (c) Confinement-induced organized swimming in three-dimensions in a coarse-grained model (248). (d) Vortices of swimming spermatozoa near a flat surface (249). (e) Active particles lead to attraction among passive colloids akin to a depletion effect (250). (f) Activity by swimming *E. coli* reduces the sedimentation speed of passive particles (251). (g) A lattice of bacterial vortices organized by an array of periodic obstacles (252). All figures reproduced with permission.

offset by a stronger hydrodynamic signal, external forces or torques on immersed bodies can generate different hydrodynamic signals as viewed far from afar. A suspension of active rollers, for instance, settles into smaller rolling groups due to long-ranged, wall-mediated interactions (256). If the rotations are instead about the wall normal, confinement can lead to peculiar effects like topologically protected edge currents and colony-scale oscillations (257–261).

New features appear as the obstacles shrink in relative size to the scale of the swimmers themselves. Active particles can produce effective attraction between passive colloids similar to a depletion effect (**Figure 12e**) (250). The sedimentation speed of passive particles can be reduced by swimming bacteria, seen in experiments with swimming *E. coli* cells and polystyrene beads (**Figure 12f**) (251). If the obstacles are fixed in space they can encourage the development of bacterial vortices just as was the case with external confinement (**Figure 12g**). With certain obstacle arrangements (Kagome lattices) such obstacles can even result in net colony rotation (252).

VIII. Large D_e , large B_n , large ϕ : many swimmers near a large deformable obstacle

In Type VIII systems the deformation of large boundaries are again substantial to the point that they can affect the behavior of a suspension of swimming cells. We have already seen that confinement of active suspensions can encourage the emergence of directed motion of a bulk suspension. But when the confinement is deformable, the relaxation timescale and associated surface tractions are strongly coupled to the dynamics of the suspension. Among other physical phenomena this territory includes moving droplets of active matter.

As in Type IV systems some of the most common deformable boundaries are fluid-air and fluid-fluid interfaces. When sufficiently many bacteria adhere to an interface they may form biofilms, introducing to the interface elastic properties which depend on the

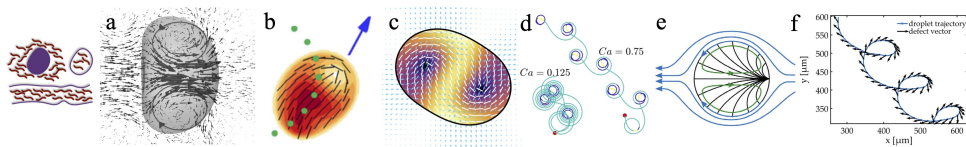


Figure 13

Type VIII systems. (a) A broken symmetry with non-motile stress-generating particles under soft confinement leads to swimming (262). (b) Zigzagging of an active nematic droplet (263). (c,d) Periodic wobbling and a transition to swimming modes of a coarse-grained non-motile suspension, tuned by the capillary number Ca (264). (e,f) Marangoni stresses on the surface of a liquid-crystal droplet couple to internal elastic modes resulting in coherent swimming, while additional symmetry-breaking results in chiral trajectories (265). All figures reproduced with permission.

strain of bacteria (173, 266). Bacteria-laden interfaces can also play an emulsion-stabilizing role similar to surfactants (267) and may render the surface viscoelastic (268). Once a biofilm is formed the relevance of swimming diminishes, but the behavior of planktonic (freely swimming) bacteria near these surfaces can impact its spread into new territories and whether the biofilm forms at all (269). Such biofilms can disrupt natural medical function, for instance in persistent infections like endocarditis (270), or can be useful for applications such as bioremediation and biodegradation.

More recent advances have considered the captivating dynamics of active droplets: active suspensions with compliant, mobile confinement. Non-motile suspensions of particles which exert an extensile stress on the surrounding fluid are known to produce large-scale flows and features similar to the swimming systems described in Type V (271). But when confined inside a droplet the resulting interaction with the boundary can lead to geometric symmetry breaking and swimming motion (**Figure 13a**) (262). More intricate dynamics are accessed by tuning the relative size of the droplet; and active nematic model showed periodic changes in alignment and stretching directions resulting in zigzag trajectories (**Figure 13b**) (263, 272). A coarse-grained model was used to reveal additional contributions of internal director field oscillations, and an array of different trajectories depending on the size of the surface tension relative to the internal stress contributions (**Figure 13c,d**) (264).

Active droplets present a curious question of placement for the classification system, as will always be the case when multiple important scales are present. When droplets move as a consequence of active internal stresses, what is more central, the self-transporting suspension dynamics at the microscale, or the net effect resulting in what appears to be a single swimmer at a much larger scale? We have included these systems in Type VIII due to the critical importance of the boundary deformability, but in this case the boundary might be considered the swimmer itself. **Figure 13e** shows a schematic for how Marangoni stresses on the surface of a liquid crystal droplet can couple to internal elastic modes, resulting in coherent swimming, along with observed chiral trajectories (**Figure 13f**) (265). For a broader discussion of active droplets see the review by Maass et al. (273).

3. SUMMARY AND OUTLOOK

We have described a proposed classification for swimming in complex fluids. The organization is based on the relationship of a swimming body to one or many obstacles in a fluid,

broadly interpreted, be they molecular fluid constituents or enormous confining boundaries. The relative length and time scales of the swimmers and obstacles, along with the concentration of swimmers, impacts the key physical principles at play and behaviors observed. We hope that this classification not only organizes the vast research that has been done, but also helps to highlight connections among research areas and those which are in need of more attention.

Within this classification, the extremes of dimensionless parameters are the easiest to understand and to model. Among the future topics which we envision are more complete explorations of the internal boundaries of the diagram, where the length and time scales of swimmers and obstacles are comparable, and the interactions of swimmers are on the precipice of a transition from dilute to collective behavior.

Another future topic is further study of systems that do not fit within this three-dimensional classification space. For example, this classification can be viewed as the low Reynolds number region of a four dimensional space with Reynolds number as an additional axis. This classification also assumes that the swimmers and obstacles have a single dominant length scale and time scale. Also absent in the classification is the obstacle concentration. For small Bn , this concentration will determine the flow properties of the suspending medium. For large Bn , we have focused on large single (isolated) obstacles or boundaries. Depending on the system type, the obstacle concentration may be an important axis to explore.

Nearly a century of effort combining biological, physical, and mathematical perspectives has established an incredible array of detailed knowledge about swimming in complex fluids. With our first steps to understand the simplest model systems behind us, we continue on to embrace the fantastic complexity of the biological realm.

“It takes more than a knock on the head to kill a scientist,” said Benes. “All that mathematics makes the skull as hard as a rock, eh?” (17)

FUTURE ISSUES

1. Additional length- and timescales provide additional axes to explore. Inertial effects would appear along another axis related to the Reynolds number. Obstacle volume fraction is another. Some systems may have multiple important swimmer length scales, like the cell body size, the flagellum diameter, and run length of a random-walk motion. Systems may have an important timescale related to their motion as individuals but also a timescale related to dynamics of the group.
2. Many studies focus on well-controlled combinations of a single type of swimmer and a single type of complex fluid, while many applications of interest are mixtures. Heterogeneous and multi-scale systems continue to need attention.
3. Within each type, the system behavior depends on the specifics of swimmer actuation, swimming gait, and deformability. This dependence will be particularly important when seeking to understand natural biological systems and engineering new synthetic systems.
4. Systems at the boundaries between identified types are expected to combine emergent features from the extremes of the classification system. Transitions between extreme behaviors may be smooth or sudden.
5. Among the eight presented system types, Type VI systems (active suspensions in

fluids with bulk complex features) are particularly challenging and understudied, both experimentally and theoretically.

6. The areas of systems and synthetic biology have expanded our understanding of internal biological processes, including how they may change in response to their environment. Coupling these internal processes with the external complex fluid behaviors described here will be an important future direction.

DISCLOSURE STATEMENT

The authors are not aware of any affiliations, memberships, funding, or financial holdings that might be perceived as affecting the objectivity of this review.

ACKNOWLEDGMENTS

We gratefully acknowledge Gwynn Elfring for helpful conversations and for critically reading the manuscript. SES acknowledges the support of the NSF/NIH (DMS-1661900, DMR-2003819). PTU acknowledges the support of the NSF (CBET-0954445, DMS-1211665).

LITERATURE CITED

1. Galias K, Mezarli C, Voultziadou E. 2017. *Fish and Fisheries* 18:1038–1055
2. Lighthill J. 1976. *SIAM Rev.* 18:161–230
3. Lauga E, Powers T. 2009. *Rep. Prog. Phys.* 72:096601
4. Elgeti J, Winkler RG, Gompper G. 2015. *Rep. Prog. Phys.* 78:056601
5. Lauga E. 2016. *Annu. Rev. Fluid Mech.* 48:105–130
6. Gompper G, Winkler RG, Speck T, Solon A, Nardini C, et al. 2020. *J. Phys.: Condensed Matter* 32:193001
7. (Editor) Spagnolie SE. 2015. *Complex Fluids in Biological Systems*. Springer, New York, N.Y.
8. Purcell EM. 1977. *Am. J. Phys.* 45:3–11
9. Childress S. 1981. *Mechanics of Swimming and Flying*. Cambridge University Press
10. Larson RG. 1999. *The Structure and Rheology of Complex Fluids*. vol. 150. Oxford University press New York
11. Hatwalne Y, Ramaswamy S, Rao M, Simha RA. 2004. *Phys. Rev. Lett.* 92:118101
12. Ishikawa T, Pedley TJ. 2007. *J. Fluid Mech.* 588:399–435
13. Haines BM, Aranson IS, Berlyand L, Karpeev DA. 2008. *Phys. Biol.* 5:046003
14. Sokolov A, Aranson IS. 2009. *Phys. Rev. Lett.* 103:148101
15. Saintillan D. 2018. *Annu. Rev. Fluid Mech.* 50:563–592
16. Bechinger C, Di Leonardo R, Löwen H, Reichhardt C, Volpe G, Volpe G. 2016. *Rev. Mod. Phys.* 88:045006
17. Asimov I, Kleiner H, Klement O. 1966. *Fantastic voyage*. vol. 3177. Bantam
18. Reiner M. 1964. *Physics Today* 17:62
19. Brennen C, Winet H. 1977. *Ann. Rev. Fluid Mech.* 9:339–398
20. Taylor GI. 1951. *Proc. Roy. Soc. Lond. A* 209:447–461
21. Blake JR. 1971. *J. Fluid Mech.* 46:199–208
22. Leiderman K, Olson SD. 2016. *Phys. Fluids* 28:021902
23. Ho N, Leiderman K, Olson S. 2008. *J. Fluid Mech.* 864:1088–1124
24. Nganguia H, Pak OS. 2018. *J. Fluid Mech.* 855:554–573

25. Leshansky AM. 2009. *Phys. Rev. E* 80:051911
26. Jung S. 2010. *Phys. Fluids* 22:031903
27. Hewitt DR, Balmforth NJ. 2017. *J. Fluid Mech.* 828:33–56
28. Kim S, Karrila SJ. 2013. *Microhydrodynamics: Principles and selected applications*. Courier Corporation
29. Chen Y, Lordi N, Taylor M, Pak OS. 2020. *Phys. Rev. E* 102:043111
30. Hewitt D. 2022. *Science Talks* 3
31. Maladen RD, Ding Y, Li C, Goldman DI. 2009. *Science* 325:314–318
32. Hosoi A, Goldman D. 2015. *Annu. Rev. Fluid Mech* 47(1):431–453
33. Krieger MS, Spagnolie SE, Powers T. 2015. *Soft Matter* 11:9115–9125
34. Cupples G, Dyson RJ, Smith DJ. 2017. *J. Fluid Mech.* 812:501–524
35. Shi J, Powers TR. 2017. *Phys. Rev. Fluids* 2
36. Suarez SS, Pacey AA. 2006. *Hum. Reprod. Update* 12:23–37
37. Fauci LJ, Dillon R. 2006. *Annu. Rev. Fluid Mech.* 38:371–394
38. Morozov A, Spagnolie SE. 2015. In *Complex Fluids in Biological Systems*. Springer, 3–52
39. Vélez-Cordero JR, Lauga E. 2013. *J. Non-Newtonian Fluid Mech.* 199:37–50
40. Vasquez PA, Forest MG. 2015. In *Complex Fluids in Biological Systems*. Springer, 53–110
41. Gagnon DA, Keim NC, Arratia PE. 2014. *J. Fluid Mech.* 758
42. Demir E, Lordi N, Ding Y, Pak OS. 2020. *Phys. Rev. Fluids* 5:111301
43. Li G, Ardekani AM. 2015. *J. Fluid Mech.* 784
44. Park JS, Kim D, Shin JH, Weitz DA. 2016. *Soft Matter* 12:1892–1897
45. Gómez S, Godínez FA, Lauga E, Zenit R. 2017. *J. Fluid Mech.* 812
46. Man Y, Lauga E. 2015. *Phys. Rev. E* 92:023004
47. Datt C, Zhu L, Elfring GJ, Pak OS. 2015. *J. Fluid Mech.* 784
48. Ho HC, Suarez SS. 2001. *Reprod.* 122:519–526
49. Shen XN, Arratia PE. 2011. *Phys. Rev. Lett.* 106:208101
50. Ives TR, Morozov A. 2017. *Phys. Fluids* 29:121612
51. Li L, Spagnolie SE. 2015. *Phys. Fluids* 27:021902
52. Teran J, Fauci L, Shelley M. 2010. *Phys. Rev. Lett.* 104:038101
53. Thomases B, Guy RD. 2014. *Phys. Rev. Lett.* 113:098102
54. Liu B, Powers TR, Breuer KS. 2011. *PNAS* **108**:19516
55. Spagnolie SE, Liu B, Powers TR. 2013. *Phys. Rev. Lett.* 111:068101
56. Martinez VA, Schwarz-Linek J, Reufer M, Wilson LG, Morozov AN, Poon WC. 2014. *PNAS* 111:17771–17776
57. Narinder N, Gomez-Solano JR, Bechinger C. 2019. *New J. Phys.* 21:093058
58. Gomez-Solano JR, Blokhuis A, Bechinger C. 2016. *Phys. Rev. Lett.* 116:138301
59. Natale G, Datt C, Hatzikiriakos SG, Elfring GJ. 2017. *Phys. Fluids* 29:123102
60. Suarez SS, Dai X. 1992. *Biol. Reprod.* 46:686–691
61. Sznitman J, Arratia P. 2015. In *Complex Fluids in Biological Systems*. Springer, 245–281
62. Elfring GJ, Lauga E. 2015. In *Complex Fluids in Biological Systems*. Springer, 283–317
63. Li G, Lauga E, Ardekani AM. 2021. *J. Non-Newtonian Fluid Mech.* 297:104655
64. Patteson AE, Gopinath A, Arratia PE. 2016. *Curr. Opin. Colloid Interface Sci.* 21:86–96
65. Lauga E. 2007. *Phys. Fluids* 19:083104
66. Balmforth NJ, Coombs D, Pachmann S. 2010. *Q. J. Mech. Appl. Math.* **63**:267
67. Fu HC, Powers TR, Wolgemuth HC. 2007. *Phys. Rev. Lett.* 99:258101–258105
68. Fu HC, Wolgemuth CW, Powers TR. 2009. *Phys. Fluids* 21:033102
69. Elfring GJ, Goyal G. 2016. *J. Non-Newtonian Fluid Mech.* 234:8–14
70. Riley EE, Lauga E. 2014. *EPL (Europhys. Lett.)* 108:34003
71. Binagia JP, Guido CJ, Shaqfeh ESG. 2019. *Soft matter* 15(24):4836–4855
72. Riley EE, Lauga E. 2015. *J. Theor. Biol.* 382:345–355
73. Pak OS, Normand T, Lauga E. 2010. *Phys. Rev. E* 81:036312

74. Li GJ, Karimi A, Ardekani AM. 2014. *Rheologica Acta* 53:911–926
75. Binagia JP, Phoa A, Housiadas K, Shaqfeh E. 2020. *J. Fluid Mech.* 900
76. Binagia JP, Shaqfeh E. 2021. *Phys. Rev. Fluids* 6(5):053301
77. Berg H.C. & Turner L. 1979. *Nature* 278:349–351
78. Kimsey RB, A. S. 1990. *J. Infect. Dis.* 162:1205–1208
79. Zhang Y, Li G, Ardekani AM. 2018. *Phys. Rev. Fluids* 3(2):023101
80. Pak O, Zhu L, Brandt L, Lauga E. 2012. *Phys. Fluids* 24(10):103102
81. Wu Z, Chen Y, Mukasa D, Pak O, Gao W. 2020. *Chem. Soc. Rev.* 49(22):8088–8112
82. Kroo L, Binagia J, Eckman N, Prakash M, Shaqfeh E. 2022. *J. Fluid Mech.* 944
83. Venugopalan PL, Esteban-Fernández de Ávila B, Pal M, Ghosh A, Wang J. 2020. *ACS nano* 14(8):9423–9439
84. Chrétien FC. 2003. *Acta Obstet Gynecol Scand* 82:449–461
85. Wróbel JK, Lynch S, Barrett A, Fauci L, Cortez R. 2016. *J. Fluid Mech.* 792:775–797
86. Schamel D, Mark AG, Gibbs JG, Miksch C, Morozov KI, et al. 2014. *ACS nano* 8:8794–8801
87. Celli JP, Turner BS, Afdhal NH, Keates S, Ghiran I, et al. 2009. *PNAS* 106:14321–14326
88. Petrou G, Crouzier T. 2018. *Biomat. Sci.* 6(9):2282–2297
89. Fu HC, Shenoy VB, Powers TR. 2010. *Europhys. Lett.* 91:24002
90. Du J, Keener JP, Guy RD, Fogelson AL. 2012. *Phys. Rev. E* 85:036304
91. Viney C, Huber AE, Verdugo P. 1993. *Macromolecules* 26:852–855
92. Zhou S, Sokolov A, Lavrentovich OD, Aranson IS. 2014. *PNAS* 111:1265–1270
93. Mushenheim PC, Trivedi RR, Weibel DB, Abbott NL. 2014. *Biophys. J.* 107:255–265
94. Trivedi RR, Maeda R, Abbott NL, Spagnolie SE, Weibel DB. 2015. *Soft Matter* 11:8404–8408
95. De Gennes PG, Prost J. 1993. *The physics of liquid crystals*. No. 83. Oxford university press
96. Peng C, Turiv T, Guo Y, Wei QH, Lavrentovich OD. 2016. *Science* 354:882–885
97. Genkin MM, Sokolov A, Lavrentovich OD, Aranson IS. 2017. *Phys. Rev. X* 7:011029
98. Krieger MS, Spagnolie SE, Powers TR. 2019. *J. Non-Newtonian Fluid Mech.* 273:104185
99. Lin Z, Chen S, Gao T. 2021. *J. Fluid Mech.* 921:A25
100. Nayani K, Córdova-Figueroa UM, Abbott NL. 2019. *Langmuir* 36:6948–6956
101. Katz DF. 1974. *J. Fluid Mech.* 64:33–49
102. Smith DJ, Blake JR. 2009. *The Mathematical Scientist* 34:74–87
103. Bianchi S, Saglimbeni F, Di Leonardo R. 2017. *Phys. Rev. X* 7:011010
104. Kantsler V, Dunkel J, Polin M, Goldstein RE. 2013. *PNAS* 110:1187–1192
105. Brosseau Q, Usabiaga FB, Lushi E, Wu Y, Ristroph L, et al. 2021. *Soft Matter* 17:6597–6602
106. Spagnolie SE, Lauga E. 2012. *J. Fluid. Mech.* 700:1–43
107. Smith DJ, Gaffney EA, Blake JR, Kirkman-Brown JC. 2009. *J. Fluid Mech.* 621:289–320
108. Mousavi SM, Gompper G, Winkler RG. 2020. *Soft Matter* 16:4866–4875
109. Mathijssen AJ, Figueroa-Morales N, Junot G, Clément E, Lindner A, Zöttl A. 2019. *Nat. Commun.* 10:1–12
110. Chen H, Thiffeault JL. 2021. *J. Fluid Mech.* 916:A15
111. Zhu L, Lauga E, Brandt L. 2013. *J. Fluid Mech.* 726:285–311
112. Jana S, Um SH, Jung S. 2012. *Phys. Fluids* 24:041901
113. Chrispell JC, Fauci LJ, Shelley M. 2013. *Phys. Fluids* 25:e1002167
114. Rothschild LJ. 1963. *Nature (London)* 198:1221–1222
115. Berg HC, Turner L. 1990. *Biophys. J.* 58:919–930
116. Frymier PD, Ford RM, Berg HC, Cummings PT. 1995. *PNAS* 92:6195–6199
117. Lauga E, DiLuzio WR, Whitesides GM, Stone HA. 2006. *Biophys. J.* 90:400–412
118. Lushi E, Kantsler V, Goldstein RE. 2017. *Phys. Rev. E* 96:023102
119. Turner L, Ryu WS, Berg HC. 2000. *J. Bacteriol.* 182:2793–2801
120. Molaei M, Barry M, Stocker R, Sheng J. 2014. *Phys. Rev. Lett.* 113:068103
121. Buchner AJ, Muller K, Mehmood J, Tam D. 2021. *PNAS* 118
122. Llopis I, an Pagonabarraga I. 2010. *J. Non-Newt. Fluid Mech.* 165:946–952

123. Goto T, Nakata K, Baba K, Nishimura M, Magariyama Y. 2005. *Biophys. J.* 89:3771–3779
124. Giacché D, Ishikawa T, Yamaguchi T. 2010. *Phys. Rev. E* 82:056309
125. Shum H, Gaffney EA, Smith DJ. 2010. *Proc. Roy. Soc. A* 466:1725–1748
126. Elgeti J, Kaupp UB, Gompper G. 2010. *Biophys. J.* 99:1018–1026
127. Hill J, Kalkanci O, McMurry JL, Koser H. 2007. *Phys. Rev. Lett.* 98:068101
128. Figueroa-Morales N, Mino GL, Rivera A, Caballero R, Clément E, et al. 2015. *Soft matter* 11(31):6284–6293
129. Ishimoto K, Crowdy DG. 2017. *J. Fluid Mech.* 821:647–667
130. Li G, Tang JX. 2009. *Phys. Rev. Lett.* 103:078101
131. Schaar K, Zöttl A, Stark H. 2015. *Phys. Rev. Lett.* 115:038101
132. Tokárová V, Perumal AS, Nayak M, Shum H, Kašpar O, et al. 2021. *PNAS* 118
133. Crowdy DG, Or Y. 2010. *Phys. Rev. E* 81:036313
134. Or Y, Zhang S, Murray RM. 2011. *SIAM J. Appl. Dyn. Sys.* 10:1013–1041
135. Zöttl A, Stark H. 2012. *Phys. Rev. Lett.* 108:218104
136. Spagnolie SE, Wahl C, Lukasik J, Thiffeault JL. 2017. *Physica D* 341:33–44
137. Liu B, Breuer KS, Powers TR. 2014. *Phys. Fluids* 26:011701
138. LaGrone J, Cortez R, Fauci L. 2019. *Phys. Rev. Fluids* 4:033102
139. Lebois F, Sauvage P, Py C, Cardoso O, Ladoux B, et al. 2012. *Biophys. J.* 102:2791–2798
140. Takagi D, Palacci J, Braunschweig AB, Shelley MJ, Zhang J. 2014. *Soft Matter* 10:1784–1789
141. Sipoš O, Nagy K, Di Leonardo R, Galajda P. 2015. *Phys. Rev. Lett.* 114:258104
142. Spagnolie SE, Moreno-Flores GR, Bartolo D, Lauga E. 2015. *Soft Matter* 11:3396–3411
143. Makarchuk S, Braz VC, Araújo NA, Ciric L, Volpe G. 2019. *Nat. Commun.* 10:1–12
144. Wykes MSD, Zhong X, Tong J, Adachi T, Liu Y, et al. 2017. *Soft Matter* 13:4681–4688
145. Mathijssen AJTM, Jeanneret R, Polin M. 2018. *Phys. Rev. Fluids* 3:033103
146. Alonso-Matilla R, Chakrabarti B, Saintillan D. 2019. *Phys. Rev. Fluids* 4:043101
147. Brown AT, Vladescu ID, Dawson A, Vissers T, Schwarz-Linek J, et al. 2016. *Soft Matter* 12:131–140
148. Bhattacharjee T, Datta SS. 2019. *Nat. Commun.* 10:1–9
149. Park S, Hwang H, Nam SW, Martinez F, Austin RH, Ryu WS. 2008. *PLoS one* 3:e2550
150. Wysocki A, Elgeti J, Gompper G. 2015. *Phys. Rev. E* 91:050302
151. Contino M, Lushi E, Tuval I, Kantsler V, Polin M. 2015. *Phys. Rev. Lett.* 115:258102
152. Mozaffari A, Sharifi-Mood N, Koplik J, Maldarelli C. 2016. *Phys. Fluids* 28:053107
153. Lintuvuori JS, Brown AT, Stratford K, Marenduzzo D. 2016. *Soft Matter* 12:7959–7968
154. Galajda P, Keymer J, Chaikin P, Austin R. 2007. *J. Bacteriol.* 189:8704–8707
155. Mueller P, Thiffeault JL. 2017. *Phys. Rev. Fluids* 2(1):013103
156. Lin Z, Thiffeault JL, Childress S. 2011. *J. Fluid Mech.* 669:167–177
157. Shum H, Yeomans JM. 2017. *Phys. Rev. Fluids* 2:113101
158. Kamdar S, Shin S, Leishangthem P, Francis LF, Xu X, Cheng X. 2022. *Nature* 603(7903):819–823
159. Majmudar T, Keaveny EE, Zhang J, Shelley MJ. 2012. *J. Roy. Soc. Interface* 9(73):1809–1823
160. Morse M, Huang A, Li G, Maxey MR, Tang JX. 2013. *Biophys. J.* 105:21–28
161. Lopez D, Lauga E. 2014. *Phys. Fluids* 26:400–412
162. Deng J, Molaei M, Chisholm NG, Stebe KJ. 2020. *Langmuir* 36:6888–6902
163. Sprenger AR, Shaik VA, Ardekani AM, Lisicki M, Mathijssen AJTM, et al. 2020. *Euro. Phys. J. E* 43:1–18
164. Crowdy D, Lee S, Samson O, Lauga E, Hosoi AE. 2011. *J. Fluid Mech.* 681:24–47
165. Dias MA, Powers TR. 2013. *Phys. Fluids* 25:101901
166. Ledesma-Aguilar R, Yeomans JM. 2013. *Phys. Rev. Lett.* 111:138101
167. Conrad JC. 2020. *J. Ind. Microbiol. Biotechnol.* 47:725–738
168. Mathijssen AJ, Doostmohammadi A, Yeomans JM, Shendruk TN. 2016. *J. Fluid Mech.* 806:35–70

169. Lemelle L, Palierne JF, Chatre E, Place C. 2010. *J. Bacteriol.* 192:6307–6308
170. Bianchi S, Saglimbeni F, Frangipane G, Dell'Arciprete D, Di Leonardo R. 2019. *Soft Matter* 15:3397–3406
171. Di Leonardo R, Dell'Arciprete D, Angelani L, Iebba V. 2011. *Phys. Rev. Lett.* 106:038101
172. Pimponi D, Chinappi M, Gualtieri P, Casciola CM. 2016. *J. Fluid Mech.* 789:514–533
173. Desai N, Shaik VA, Ardekani AM. 2018. *Soft Matter* 14:264–278
174. Shaik VA, Ardekani AM. 2019. *Phys. Rev. E* 99:033101
175. Ahmadzadegan A, Wang S, Vlachos PP, Ardekani AM. 2019. *Phys. Rev. E* 100:062605
176. Trouilloud R, Yu T, Hosoi A, Lauga E. 2008. *Phys. Rev. Lett.* 101:048102
177. Shaik VA, Ardekani AM. 2017. *J. Fluid Mech.* 824:42–73
178. Wu H, Thiébaud M, Hu WF, Farutin A, Rafai S, et al. 2015. *Phys. Rev. E* 92:050701
179. Dalal S, Farutin A, Misbah C. 2020. *Soft Matter* 16:1599–1613
180. Woolley DM, Crockett RF, Groom WD, Revell SG. 2009. *J. Exp. Biol.* 212:2215–2223
181. Yuan J, Raizen DM, Bau H. 2014. *PNAS* 111:6865–6870
182. Dombrowski C, Cisneros L, Chatkaew S, Goldstein RE, Kessler JO. 2004. *Phys. Rev. Lett.* 93:098103
183. Hernandez-Ortiz JP, Stoltz CG, Graham MD. 2005. *Phys. Rev. Lett.* 95:204501
184. Saintillan D, Shelley MJ. 2007. *Phys. Rev. Lett.* 99:058102
185. Evans AA, Ishikawa T, Yamaguchi T, Lauga E. 2011. *Phys. Fluids* 23:111702
186. Schoeller SF, Keaveny EE. 2018. *J. Roy. Soc. Interface* 15:20170834
187. Saintillan D, Shelley MJ. 2013. *C. R. Phys.* 14:497–517
188. Miles CJ, Evans AA, Shelley MJ, Spagnolie SE. 2019. *Phys. Rev. Lett.* 122:098002
189. Ramaswamy S. 2010. *Annu. Rev. Condens. Matter Phys.* 1:323–345
190. Koch DL, Subramanian G. 2011. *Annu. Rev. Fluid Mech.* 43:637–659
191. Vicsek T, Zafeiris A. 2012. *Phys. Rep.* 517:71–140
192. Marchetti MC, Joanny JF, Ramaswamy S, Liverpool TB, Prost J, et al. 2013. *Rev. Mod. Phys.* 85:1143
193. Saintillan D, Shelley MJ. 2015. In *Complex Fluids in Biological systems*. Springer, 319–355
194. Alert R, Casademunt J, Joanny JF. 2022. *Annu. Rev. Condens. Matter Phys.* 13:143–170
195. Bowick M, Fakhri N, Marchetti M, Ramaswamy S. 2022. *Phys. Rev. X* 12(1):010501
196. Shankar S, Souslov A, Bowick M, Marchetti MC, Vitelli V. 2022. *Nature Rev. Phys.* 4(6):380–398
197. Gachelin J, Rousselet A, Lindner A, Clement E. 2014. *New J Phys.* 16:025003
198. Patterson A, Gopinath A, Purohit PK, Arratia PE. 2016. *Soft Matter* 12(8):2365–2372
199. Peng Y, Lai L, Tai YS, Zhang K, Xu X, Cheng X. 2016. *Phys. Rev. Lett.* 116(6):068303
200. Soni V, Bililign E, Magkiriadou S, Sacanna S, Bartolo D, et al. 2019. *Nature Phys.* 15(11):1188–1194
201. Han K, Kokot G, Tovkach O, Glatz A, Aranson I, Snezhko A. 2020. *Proc. Natl. Acad. Sci.* 117(18):9706–9711
202. Petroff AP, Wu XL, Libchaber A. 2015. *Phys. Rev. Lett.* 114(15):158102
203. Tan T, Mietke A, Li J, Chen Y, Higinbotham H, et al. 2022. *Nature* 607:287–293
204. Underhill PT, Hernandez-Ortiz JP, Graham MD. 2008. *Phys. Rev. Lett.* 100:248101
205. Ishikawa T, Locsei J, Pedley T. 2008. *J. Fluid Mech.* 615:401–431
206. Underhill PT, Graham MD. 2011. *Phys. Fluids* 23:121902
207. Saintillan D, Shelley MJ. 2012. *J. Roy. Soc. Interface* 9:571–585
208. Bárdfalvy D, Nordanger H, Nardini C, Morozov A, Stenhammar J. 2019. *Soft Matter* 15:7747–7756
209. Kasyap T, Koch DL, Wu M. 2014. *Phys. Fluids* 26(8):081901
210. Morozov A, Marenduzzo D. 2014. *Soft Matter* 10(16):2748–2758
211. Stenhammar J, Nardini C, Nash RW, Marenduzzo D, Morozov A. 2017. *Phys. Rev. Lett.* 119:028005

212. Brotto T, Bartolo D, Saintillan D. 2015. *J. Nonlinear Sci.* 25:1125–1139
213. Schoeller SF, Holt WV, Keaveny EE. 2020. *Phil. Trans. Roy. Soc. B* 375:20190384
214. Simha RA, Ramaswamy S. 2002. *Phys. Rev. Lett.* 89:058101
215. Qian Y, Kramer PR, Underhill PT. 2017. *Phys. Rev. Fluids* 2:043104
216. Škultéty V, Nardini C, Stenhammar J, Marenduzzo D, Morozov A. 2020. *Phys. Rev. X* 10:031059
217. Rafai S, Jibuti L, Peyla P. 2010. *Phys. Rev. Lett.* 104:098102
218. Mussler M, Rafai S, Peyla P, Wagner C. 2013. *Europhys. Lett.* 101:54004
219. Gachelin J, Mino G, Berthet H, Lindner A, Rousselet A, Clément É. 2013. *Phys. Rev. Lett.* 110:268103
220. López HM, Gachelin J, Douarche C, Auradou H, Clément E. 2015. *Phys. Rev. Lett.* 115:028301
221. McDonnell AG, Gopesh TC, Lo J, O'Bryan M, Yeo LY, et al. 2015. *Soft Matter* 11:4658–4668
222. Saintillan D. 2010. *Phys. Rev. E* 81(5):056307
223. Guo S, Samanta D, Peng Y, Xu X, Cheng X. 2018. *Proc. Natl. Acad. Sci.* 115(28):7212–7217
224. Takatori S, Brady J. 2017. *Phys. Rev. Lett.* 118:018003
225. Ishikawa T, Brumley DR, Pedley TJ. 2021. *J Fluid Mech.* 914
226. Matsui H, Omori T, Ishikawa T. 2020. *Phys. Fluids* 32:071902
227. Bozorgi Y, Underhill PT. 2014. *Rheol. Acta* 53(12):899–909
228. Bechtel TM, Khair AS. 2017. *Rheologica Acta* 56:149–160
229. Cates M, Fielding S, Marenduzzo D, Orlandini E, Yeomans J. 2008. *Phys. Rev. Lett.* 101:068102
230. Giomi L, Liverpool TB, Marchetti MC. 2010. *Phys. Rev. E* 81:051908
231. Liu Z, Zhang K, Cheng X. 2019. *Rheol. Acta* 58(8):439–451
232. Hochbaum AI, Aizenberg J. 2010. *Nano letters* 10:3717–3721
233. Tung CK, Lin C, Harvey B, Fiore AG, Ardon F, et al. 2017. *Sci. Rep.* 7:1–9
234. Sokolov A, Zhou S, Lavrentovich OD, Aranson IS. 2015. *Phys. Rev. E* 91:013009
235. Zhou S, Tovkach O, Golovaty D, Sokolov A, Aranson IS, Lavrentovich OD. 2017. *New J. Phys.* 19:055006
236. Liu S, Shankar S, Marchetti MC, Wu Y. 2021. *Nature* 590:80–84
237. Bozorgi Y, Underhill PT. 2014. *J. Non-Newtonian Fluid Mech.* 214:69–77
238. Li G, Ardekani AM. 2016. *Phys. Rev. Lett.* 117:118001
239. Elfring GJ, Pak OS, Lauga E. 2010. *J. Fluid Mech.* 646:505
240. Bozorgi Y, Underhill PT. 2011. *Phys. Rev. E* 84:061901
241. Bozorgi Y, Underhill PT. 2013. *J. Rheology* 57:511
242. Li G, Ardekani AM. 2016. *Phys. Rev. Lett.* 117:118001
243. Caldara M, Friedlander RS, Kavanaugh NL, Aizenberg J, Foster KR, Ribbeck K. 2012. *Curr. Biol.* 22:2325–2330
244. Wagner CE, Wheeler KM, Ribbeck K. 2018. *Annu. Rev. Cell Dev. Biol.* 34:189–215
245. Lushi E, Wioland H, Goldstein RE. 2014. *PNAS* 111:9733–9738
246. Wioland H, Woodhouse FG, Dunkel J, Goldstein RE. 2016. *Nat. Phys.* 12:341–345
247. Wioland H, Lushi E, Goldstein RE. 2016. *New J. Physics* 18:075002
248. Theillard M, Saintillan D. 2019. *J. Comput. Phys.* 397:108841
249. Riedel IH, Kruse K, Howard J. 2005. *Science* 309:300–303
250. Angelani L, Maggi C, Bernardini ML, Rizzo A, Di Leonardo R. 2011. *Phys. Rev. Lett.* 107:138302
251. Singh J, Patteson AE, Maldonado BOT, Purohit PK, Arratia PE. 2021. *Soft Matter* 17:4151–4160
252. Reinken H, Nishiguchi D, Heidenreich S, Sokolov A, Bär M, et al. 2020. *Commun. Phys.* 3:1–9
253. Theillard M, Alonso-Matilla R, Saintillan D. 2017. *Soft Matter* 13:363–375
254. Zöttl A, Stark H. 2014. *Phys. Rev. Lett.* 112:118101
255. Hernandez-Ortiz JP, Underhill PT, Graham MD. 2009. *J. Phys.: Cond. Matt.* 21:204107

256. Driscoll M, Delmotte B, Youssef M, Sacanna S, Donev A, Chaikin P. 2017. *Nature Phys.* 13:375–379
257. van Zuiden BC, Paulose J, Irvine WTM, Bartolo D, Vitelli V. 2016. *Proc. Natl. Acad. Sci.* 113(46):12919–12924
258. Dasbiswas K, Mandadapu KK, Vaikuntanathan S. 2018. *Proc. Natl. Acad. Sci.* 115(39):E9031–E9040
259. Yang X, Ren C, Cheng K, Zhang H. 2020. *Physical Review E* 101(2):022603
260. Liu P, Zhu H, Zeng Y, Du G, Ning L, et al. 2020. *Proc. Natl. Acad. Sci.* 117(22):11901–11907
261. Zhang B, Hilton B, Short C, Souslov A, Snezhko A. 2020. *Phys. Rev. Research* 2(4):043225
262. Tjhung E, Marenduzzo D, Cates ME. 2012. *PNAS* 109:12381–12386
263. Gao T, Li Z. 2017. *Phys. Rev. Lett.* 119:108002
264. Young YN, Shelley MJ, Stein DB. 2021. *Math. Biosci. Eng.* 18:2849–2881
265. Krüger C, Klös G, Bahr C, Maass CC. 2016. *Phys. Rev. Lett.* 117:048003
266. Vaccari L, Molaei M, Niepa TH, Lee D, Leheny RL, Stebe KJ. 2017. *Adv. Colloid Interface Sci.* 247:561–572
267. Dorobantu LS, Yeung AK, Foght JM, Gray MR. 2004. *Appl. Env. Microbiol.* 70:6333–6336
268. Rivas DP, Hedgecock ND, Stebe KJ, Leheny RL. 2021. *Soft Matter* 17:8195–8210
269. Mazza MG. 2016. *J. Physics D: Applied Physics* 49(20):203001
270. Costerton JW, Stewart PS, Greenberg EP. 1999. *science* 284:1318–1322
271. Sanchez T, Chen DTN, DeCamp SJ, Heymann M, Dogic Z. 2012. *Nature* 491:431–434
272. Whitfield CA, Hawkins RJ. 2016. *New J. Phys.* 18:123016
273. Maass CC, Krüger C, Herminghaus S, Bahr C. 2016. *Annu. Rev. Cond. Mat. Phys.* 7:171–193